# Ice-Nucleating Particles Near Two Major Dust Source Regions

Charlotte M. Beall[1,2], Thomas C. J. Hill[3], Paul J. DeMott[3], Tobias Köneman[2*], Michael Pikridas[4], Frank Drewnick[5], Hartwig Harder[6], Christopher Pöhlker[2], Jos Lelieveld[4,6], Bettina Weber[2**], Minas Iakovides[4], Roman Prokeš[7,8], Jean Sciare[4], Meinrat O. Andreae[1,2,9], M. Dale Stokes[1], Kimberly A. Prather[1,10]

[1]Scripps Institution of Oceanography, University of California San Diego, La Jolla, CA 92037, USA

[2]Max Planck Institute for Chemistry, Multiphase Chemistry and Biogeochemistry Departments, D-55128 Mainz, Germany

[3]Department of Atmospheric Science, Colorado State University, Fort Collins, CO 80523, USA

[4]Climate & Atmosphere Research Center, The Cyprus Institute, Nicosia, CY-1645, Cyprus

[5] Max Planck Institute for Chemistry, Particle Chemistry Department, D-55128 Mainz, Germany

[6]Max Planck Institute for Chemistry, Atmospheric Chemistry Department,
D-55128 Mainz, Germany

[7]RECETOX, Faculty of Science, Masaryk University, Kotlarska 2, 611 Brno, Czech Republic

[8]Department of Atmospheric Matter Fluxes and Long-range Transport, Global Change Research Institute of the Czech Academy of Sciences, Belidla 4a, 60300, Brno, Czech Republic

[9]Department of Geology and Geophysics, King Saud University, Riyadh, Saudi Arabia

[10]Department of Chemistry and Biochemistry, University of California San Diego, La Jolla, CA, 92093 USA

*Now at Envicontrol GmbH, Waidmarkt 11, 50676 Köln, Germany

**Now at: Institute of Biology, University of Graz, 8010 Graz, Austria

*Correspondence to: Charlotte M. Beall, cbeall@ucsd.edu*

## Abstract

Mineral dust and sea spray aerosol represent important sources of ice-~~-~~nucleating particles (INPs), the minor fraction of aerosol particles able to trigger cloud ice crystal formation and, consequently, influence multiple climate-relevant cloud properties including lifetime, ~~reflectivity,~~radiative properties and precipitation initiation efficiency. Mineral dust is considered the dominant INP source in many parts of the world due to its ice nucleation efficiency and its sheer abundance, with global emission rates of up to 4700 Tg $a^{-1}$. However, INPs emitted from the ocean surface in sea spray aerosol frequently dominate INP populations in remote marine environments, including parts of the Southern Ocean where cloud-resolving model simulations have demonstrated that cloud ~~reflectivity is~~radiative properties are likely strongly controlled by INPs. Here we report INP concentrations measured in aerosol and seawater samples during Air Quality and Climate Change in the Arabian BAsin (AQABA), a shipborne campaign that spanned the Red Sea, Gulf of Aden, Arabian Sea, Arabian Gulf, and part of the Mediterranean. In aerosol samples collected within a few hundred kilometers of the first and second ranked sources of dust globally, the Sahara and Arabian Peninsula, INP concentrations ranged from 0.2 to 11 $L^{-1}$ at -20 °C with observed ice-active surface ~~nucleation~~ site densities ($n_s$) 1-3 orders of magnitude below levels predicted by mineral dust INP parameterizations. Over half of the samples (at least 14 of 26) were collected during dust storms with average dust mass concentrations between 150 and 490 μg $m^{-3}$ ($PM_{10}$), as simulated by the Modern-Era Retrospective analysis for Research and Application, version 2 (MERRA-2). The impacts of heat and peroxide treatments indicate that organics ~~were responsible for~~dominated the observed ice nucleation (IN) -activity at temperatures ≥ -15 °C with proteinaceous (heat-labile) INPs frequently observed at high~~er~~ freezing temperatures > -10 °C. INP concentrations in seawater samples ranged between 3 and 46 $mL^{-1}$ at -19 °C, demonstrating the relatively low INP source potential of seawater in the region as compared to seawater from multiple other regions reported previously. Overall, our results demonstrate that despite proximity to the Sahara and the Arabian Peninsula and the dominance of mineral dust in the aerosol sampled, existing mineral dust parameterizations alone would not skillfully represent the near-surface $n_s$ in the observed temperature regime (-6 to -25 °C). ~~The decreased $n_s$, and results demonstrating that organics dominated the observed IN activity > -15 °C, indicate that the IN active organic species are limited compared to the mineral IN components of dust.~~ Future efforts to develop or improve representations of dust INPs at modest supercooling (≥~~>~~-15 °C) would benefit from a characterization of the specific organic species associated with dust INPs. More generally, an improved understanding of the organic species associated with increased IN -activity and their variability across dust source regions would directly inform efforts to determine whether $n_s$-based parameterizations are appropriate for faithful representation of dust

**Formatted:** Font: (Default) Times New Roman

**Formatted:** Font: (Default) Times New Roman, 11 pt

**Formatted:** Font: 11 pt

**Formatted:** Font: (Default) Times New Roman, 11 pt

INPs in this sensitive temperature regime, whether region-specific parameterizations are required, or whether an alternative to the $n_s$ approach is necessary.

Formatted: Font color: Black

## 1 Introduction

Ice-nucleating particles (INPs) modulate the temperature and relative humidity at which ice particle formation occurs in the atmosphere and thus are a key factor that controls ice-phase partitioning in clouds. As initiators of ice formation and related phase-partitioning processes, INPs affect multiple cloud properties and exert a strong influence on cloud lifetime, ~~reflectivity~~ radiative properties and precipitation initiation efficiency (e.g. Lohmann and Feichter, 2005; Vergara-Temprado et al., 2018~~);~~ ~~(~~Brunner et al., 2021).

Globally, desert dust is likely the most abundant aerosol type by mass (Kinne et al., 2006; Kok et al., 2021). Furthermore, multiple studies have demonstrated that mineral dust is the dominant ice-nucleating ~~(IN)~~ species in many parts of the world based on observations (Ardon-Dryer and Levin, 2014; Boose et al., 2016; DeMott et al., 2015a; Price et al., 2018) and modeling of global INP distributions (Burrows et al., 2013; Hoose et al., 2010; Murray et al., 2012; Vergara-Temprado et al., 2017). Annual global dust emission rate estimates range between 400 and 4700 Tg $a^{-1}$ (Huneeus et al., 2011; Kok et al., 2021). Of the average global dust loading in the atmosphere (20-29 Tg), North African source regions are estimated to contribute ~50% (11-15 Tg), and the Middle East and Central Asian source regions account for the bulk of the remainder, ~30% (7.7 Tg) (Kok et al., 2021). Analysis of satellite products indicates that dust emission~~s~~ rates are increasing over the Middle East at a rate of 15% $a^{-1}$ (Klingmüller et al., 2016; Yu et al., 2018).

While Hoose and Möhler (2012) showed that mineral dust INPs generally activate ice crystals at freezing temperatures < -15 °C, dust containing K-feldspar has been shown to nucleate ice at much warmer temperatures, up to -4 °C (Atkinson et al., 2013; Harrison et al., 2016; Niedermeier et al., 2015; Wex et al., 2014; Whale et al., 2015; Zolles et al., 2015). K-feldspars represent up to ~24% of Saharan and Asian dusts by mass (Nickovic et al., 2012). However, knowledge of the abundance and the available surface fraction of aerosolized K-feldspar would be necessary to evaluate the IN efficiency of dust at temperatures > -15 °C (Kanji et al., 2017).

Though mineral dust is considered to be the dominant INP source in many regions, multiple modeling and observational studies suggest that marine INPs are frequently dominant by number

in remote ocean regions in air masses with low concentrations of terrestrial aerosol (McCluskey et al., 2018b, 2018c; Vergara-Temprado et al., 2017; Wilson et al., 2015; DeMott et al., 2016). Using a global aerosol model to simulate marine organic and K-feldspar INP populations, Vergara-Temprado et al. (2017) showed that the relative contribution of marine organic vs. dust INPs in remote regions varies seasonally, and that marine organic INPs frequently outnumber K-feldspar INPs (up to 100% of the simulated days in the Southern Ocean during summer). Results from a follow-on cloud-resolving model study showed that Southern Ocean cloud reflectivity is strongly modulated by INP concentrations, indicating that accurate estimates of the radiative energy budget in the Southern Ocean likely require improved and reliable representation of both dust and marine organic INPs (Vergara-Temprado et al., 2018). By generating isolated nascent sea spray aerosol over a range of biological conditions, mesocosm studies have shown that marine INPs are comprised of two classes: a dissolved organic carbon (DOC) type composed of IN-active molecules and a particulate organic carbon (POC) type linked to the death phase of phytoplankton blooms (McCluskey et al., 2017, 2018b).

Parameterizations for both marine and mineral dust populations are commonly implemented in atmospheric models to estimate dust and marine INP concentrations. There are multiple existing mineral dust INP parameterizations used to estimate their concentrations in aerosolized desert dust, some based exclusively on laboratory measurements (e.g., Niemand et al., 2012; Ullrich et al., 2017), and others derived from a combination of laboratory and field measurements (DeMott et al., 2015). There are, additionally, multiple mineral-specific INP parameterizations including illite (Broadley et al., 2012), kaolinite (Welti et al., 2012), quartz (Harrison et al., 2019) and K-feldspar (Atkinson et al., 2013; hereafter, "A13"). The parameterizations by Ullrich et al. (2017;~~,~~ hereafter, "U17") and Niemand et al. (2012;~~,~~ hereafter, "N12") were developed using dust samples from multiple deserts, and both found little variability in the IN activity between dusts from locations as disparate as the Sahara and Asia. DeMott et al. (2015;~~,~~ hereafter, "D15") found agreement between their observations-based parameterization and N12, supporting the validity of laboratory-based parameterizations. Results in D15 also confirmed the conclusions of N12 and U17: that to first order, dusts from distinct regions can be parameterized as a single particle type. The D15 parameterization has been considered to be representative of dust that has undergone atmospheric photochemical and oxidative processes in transport (i.e., "aged" dust), because the

parameterization was derived from observations made far (1000s of kilometers) from the dust emissions sources (Boose et al., 2016).

By contrast, few studies report *in situ* INP measurements near (e.g., < 1 day of transport) a major dust source, and the lack of observations near dust source regions inhibit the evaluation of the ability of existing dust INP parameterizations to represent nascent dust populations (Boose et al., 2016; Gong et al., 2020; Price et al., 2018). INP observations are particularly lacking for the sensitive temperature regime > -20 °C. Boose et al. (2016) found that D15 overpredicted INPs observed during Saharan dust events at a location within 100s of km west of the Sahara (Izaña, Tenerife, Spain) by 2-3 orders of magnitude, suggesting that aging may lead to increased IN efficiency in mineral dust and that D15 may be less representative of nascent dust. These conclusions were supported by Conen et al. (2015), who found that concentrations of INPs at -20 °C measured during Saharan dust events were one order of magnitude higher at Jungfraujoch in the Swiss Alps than in Izaña, where dust events had occurred 1-7 d prior to reaching Jungfraujoch. Gong et al. (2020) measured INPs in a variety of atmospheric and seawater sample types at Cabo Verde and determined mineral dust to be the dominant source of INPs observed in the atmosphere but found that INPs with freezing temperatures > -10 °C were likely biological. At altitudes between 30 and 3500 m in the same region, Price et al. (2018) found that measured concentrations of INPs ranged two orders of magnitude at a given temperature, and that the observed concentrations related to the atmospheric dust loadings.

Recently, multiple studies have provided new, much-needed observations of ambient atmospheric INPs in marine environments (DeMott et al., 2016; Hartmann et al., 2020; McCluskey et al., 2018c, 2018d; Yang et al., 2020) where data was historically lacking and, consequently, an impediment to achieving predictive understanding of global INP distributions (Burrows et al., 2013). There are now two parameterizations available for the estimation of atmospheric concentrations of marine INPs emitted from the ocean surface: Wilson et al. (2015), which estimates cumulative INPs from total organic carbon (TOC) concentrations in simulated sea spray aerosol (SSA), and McCluskey et al. (2018), which estimates ice-active surface ~~nucleation~~ site density ($n_s$) from aerosol surface area. Wilson et al. (2015) and McCluskey et al. (2018; hereafter "M18") derived marine INP parameterizations from field measurements of INPs in Atlantic and Arctic Ocean sea surface microlayer samples and pristine SSA samples over the North Atlantic Ocean, respectively.

Formatted: Font: Italic

Here, we report observations of INPs measured in air masses influenced by both desert dust and marine aerosol (Edtbauer et al., 2020) in close proximity to the two greatest global dust aerosol sources: the Sahara (#1) and the Arabian Peninsula (#2) (Kok et al., 2021). INP concentrations were measured in 26 ambient aerosol samples collected during Air Quality and Climate Change in the Arabian Basin (AQABA), a shipborne campaign which took place July – August 2017 on a transect that spanned the ~~-~~central and eastern parts of the Mediterranean, the Red Sea, the Gulf of Aden, the Arabian Sea and the Arabian Gulf. The rest of this study will be structured as follows. We present an overview of measurements and data sources in Sect. 2 Methods. In Results Sect. 3.1, an overview of INP concentrations observed is presented, followed by an assessment of subsurface seawater (SSW) source potential (Sect. 3.2). ~~Observed~~Observed $n_s$ ~~were~~ are compared to dust and marine INP parameterizations in Sect. 3.3, followed by an analysis of the~~, and the~~ contributions of heat-labile (e.g., proteinaceous) and heat-stable organic compounds to observed INP populations in aerosol (Sect. 3.4). The same analysis is applied to assess organic contributions to observed INPs in a soil dust sample from a likely source region in Sect. 3.5. We discuss the findings, potential INP sources and compare with prior studies in the Discussion Sect. 5. Finally, in Sect. 5 we offer strategies to address the challenges of evaluating dust-specific INP parameterizations and recommend measurements needed to develop predictive understanding of dust INPs at modest supercooling ($T \geq 15$°C). ~~were assessed via heat and peroxide treatments. Finally, the potential INP source strengths of subsurface seawater (SSW) were assessed and compared with SSW INP measurements from prior studies of remote and coastal seawater.~~

## 2 Methods

### 2.1 Project Overview

The AQABA campaign was conducted from 25 June to 3 September 2017 onboard the RV *Kommandor Iona*. The research voyage was conducted in two transects: the first leg beginning in La-Seyne-sur-Mer, France, heading through the Suez Canal, around the Arabian Peninsula and ending in Kuwait, and second leg a return transect via the same route (Figs. S1-S2). The campaign supported a large suite of on- and offline aerosol and gas-phase measurements (Bourtsoukidis et

al., 2019, 2020; Celik et al., 2020; Edtbauer et al., 2020; Eger et al., 2019; Friedrich et al., 2021; Pfannerstill et al., 2019; Tadic et al., 2020; Wang et al., 2020).

### 2.2 Aerosol and Trace Gas Measurements

Aerosol size distributions were measured using an Optical Particle Spectrometer (OPC, Grimm model 1.109) and a Fast Mobility Particle Spectrometer (FMPS, TSI model 3091). The OPC measures particles in the size range 0.25 – 32 µm, and the FMPS measures particles with sizes between 5.6 nm and 560 nm with 6s and 1s time resolution, respectively. The inlet for the aerosol instrumentation was located at the top of a measurement container at a horizontal distance of about 15~~25~~ m from the INP filter sampling unit (Figs. S3-S4). To avoid condensation in inlet lines, aerosol samples were passed through a drying system, which reduced ambient relative humidity (RH) to an average value of ≈ 40 % in the measurement container. Ambient RH ranged between 67 and 81% during INP sampling periods. OPC and FMPS data were averaged over 1-minute time intervals. A filter flag based on aerosol measurements was derived to identify and eliminate stack emissions and applied to all aerosol data. The filter flag was based on short term variation in particle number concentration measured by a Condensation Particle Counter (CPC, TSI model 3787), black carbon concentrations (Aethalometer, Magee AE33), wind direction and speed. The flag was set when the apparent wind direction was from the direction of the stack (± 30°) as seen from the aerosol inlet position (Fig. S3) and strong fluctuations of black carbon and/or particle number concentrations were observed relative to background levels. ~~Two additional measurements provided aerosol data from which a filter flag intended to identify and eliminate stack emissions was derived: particle number concentrations as measured by a Condensation Particle Counter (CPC, TSI model 3787) and black carbon concentrations (Aethalometer, Magee AE33). The filter flag, based on short term variation in particle number concentration, black carbon concentration, wind direction and speed, was applied to all aerosol data so that samples contaminated by stack emissions could be identified.~~ Particle losses were estimated using the Particle Loss Calculator (von der Weiden et al., 2009). Losses were negligible (<1%) up to 3.5 µm and increased to 40% at 10 µm.

Particle surface area concentrations were derived from the 1-min time-averaged FMPS and OPC measurements as follows. Geometric diameters were estimated from the measured mobility

Formatted: Font: Not Bold
Formatted: Font: Not Bold
Formatted: Font: Not Bold
Formatted: Font: Not Bold
Formatted: Font: Not Bold
Formatted: Font: Not Bold
Formatted: Font: Not Bold
Formatted: Font: Not Bold

diameters (FMPS) and optical particle diameters (OPC). Aerosols were assumed dry at sampling conditions following the drying system described above. To convert optical particle diameters into geometric diameters, it was assumed that all coarse particles ($d_p$ > 3000 nm) were composed of sea salt and dust with a mass ratio of 25% to 75%, and ~~for~~ using the respective refractive indices and shapes the measured optical particle diameters were converted into geometric diameters (Sect. S1.1). The sea salt:dust mass ratio was based on average dust and sea salt concentrations as measured in particles < 10 µm ($PM_{10}$; see Sect. S2 for details).

Fine particle ($d_p$ < 700 nm) size~~s were~~ was converted from optical diameter ($d_{opt}$) into geometric diameter ($d_{geo}$) using the optical properties calculated from the ~~$PM_1$~~ chemical composition of particles < 1 µm ($PM_1$) as measured by an Aerosol Mass Spectrometer (Aerodyne HR-ToF-AMS), assuming spherical particles ~~( Celik et al., 2020)~~. For particles in the intermediate size range (700 – 3000 nm), log-linear interpolation of optical and spherical properties was applied for conversion of optical into geometric particle diameters (Sect. S1.2). The mobility diameters measured by the FMPS were considered equivalent to the geometric diameter, assuming spherical particles. From the resulting particle size distributions, particle surface area was calculated for each size bin. Total particle surface concentrations were determined by integrating the surface area distribution for particles up to 10 µm ($d_{geo}$). The overall uncertainty of derived particle surface area concentrations is estimated to be 30%, including the uncertainty due to particle losses (see Sect. S3).

The water-soluble fraction of total suspended particles (TSPs) was monitored with hourly resolution using a Monitor for AeRosols and Gases in Ambient Air, MARGA (Metrohm Applikon model S2, Herisau, Switzerland). Sea salt concentrations were estimated by scaling measured soluble $Na^+$ concentrations by 3.27 following Manders et al. (2009) and were used as a proxy for SSA number concentrations. Size-resolved single particle chemical composition measurements have shown that sea salt represents 50-70% of SSA particles by number ($d_p$ > 0.5µm) (Collins et al., 2014). ~~-~~Hourly composition data was linearly interpolated for 4 samples where 1-3 hours (of 7-24 hours total sampling time) was missing (Fig. S~~5~~3). The MARGA sampling line was equipped with a $PM_{10}$ cyclone, but the sample was not dried as the instrument is not prone to

Formatted: Font: Not Bold
Formatted: Font: Not Bold
Formatted: Font: Not Bold
Formatted: Font: Not Bold
Formatted: Font: Not Bold, Subscript
Formatted: Not Superscript/ Subscript
Formatted: Not Superscript/ Subscript
Formatted: Font: Not Bold
Formatted: Not Superscript/ Subscript
Formatted: Not Superscript/ Subscript
Formatted: Subscript
Formatted: Font: Not Bold
Formatted: Font: Not Bold, Subscript
Formatted: Font: Not Bold
Formatted: Font: Not Bold

condensation. Particle transmission losses to the MARGA were estimated using the PLC and found to be consistent with the aerosol sizing instruments described above.

Nitric oxide (NO) concentrations were measured using a commercially available two-channel chemiluminescence monitor, CLD 790 SR (ECO Physics AG, Dürnten, Switzerland). During the AQABA campaign, the CLD 790 SR, MARGA, FMPS, OPC, HR-ToF-AMS, CPC and Aethalometer were operated within laboratory containers on the main deck of the research vessel. The NO measurements were used to prevent stack sampling during INP collection (see Sect. 2.4).

### 2.3 Dust Mass Concentrations from MERRA-2

~~Area-averaged h~~Since dust concentrations were not measured during the campaign, hourly dust surface mass concentrations along the cruise track were obtained from the (0.5 ~~×~~ 0.625 °) Modern-Era Retrospective analysis for Research and Application, version 2 (MERRA-2; Gelaro et al., 2017) and were averaged over the region covered during each sampling period. ~~(~~Buchard et al.~~,~~ ~~(~~2017) showed a high degree of correlation between MERRA-2 and surface dust concentration observations ($r \geq 0.69$), particularly during dust storms ($r \geq 0.92$). MERRA-2 surface dust mass concentrations also correlated well with $PM_{10}$ observed during AQABA ($r \geq 0.71$) (Fig. S6). MERRA-2 uses the GEOS-5 Earth system model (Molod et al., 2015; Rienecker et al., 2011) with 72 vertical layers between the surface and 0.01 hPa (~ 80 km) and the three-dimensional variational data assimilation Gridpoint Statistical Interpolation analysis system (Kleist et al., 2009; Wu et al., 2002, additional details in Sect. S4). ~~It simulates 5 types of aerosols (dust, sea salt, sulfate and black and organic carbon) using the Goddard Chemistry, Aerosol, Radiation, and Transport (GOCART) model (Chin et al., 2002; Colarco et al., 2010). Dust emissions and deposition rates in MERRA-2 are estimated by summing the emissions and deposition rates across GOCART simulated dust particles between 0.1 – 10 μm in size (dry diameter) (Gelaro et al., 2017). Dust emissions are constrained by wind-driven erosion over the source locations, which are identified from the topographic depression map (Ginoux et al., 2001). Aerosol observations are derived from various satellite products and are jointly assimilated within GEOS-5 with meteorological observations (Buchard et al., 2017). MERRA-2 has been shown to successfully reproduce the interannual variability of North Atlantic dust transport. Additionally, the improved aerosol~~

Formatted: Font: (Default) Times New Roman, 12 pt

Formatted: Subscript

~~assimilation scheme in MERRA-2 was shown to have a positive impact on the representation of long-range dust transport from the Sahara compared to prior versions (Buchard et al., 2017).~~

### 2.4 INP Measurements in Aerosol ~~Measurement of Ice Nucleating Particles~~

Ambient aerosol sampling for offline measurement of INPs was conducted from 5 Jul – 31 Aug 2017 on the *Kommandor Iona's* wheelhouse top (platform above the bridge), ~1~~2~~5 m horizontally from the online aerosol measurements inlet and ~1~~3~~5 m from the ocean surface (Figs. S3-4). Sampling locations along the cruise transect corresponding to each aerosol sample are shown in Figs. S1-2.

Aerosol samples were collected over 3-28 hour periods on polycarbonate filters (47 mm diameter, 0.2 µm pore-size, Whatman® Nuclepore, Chicago, Illinois, USA) placed in open-face Nalgene® Analytical Filter Units (Waltham, Massachusetts, USA). Sampling intervals and frequency were chosen with the aim of collecting > 5000 L during dust events and > 10,000 L when OPC particle counts were relatively low (e.g., during sampling periods f040-44), as conditions allowed. Aerosol sampling flow rates through the filter units were set to 10-13 ~~Lpm~~ LPM using a MassStream™ mass flow controller (Bethlehem, PA, USA) connected inline with a rotary vane pump (Thomas QR-0100, Gardner Denver ©, Monroe, LA, USA). To decrease exposure to stack emissions, the pump was automated to switch off when online measurements of NO exceeded one standard deviation above the average background concentration for over 1 minute (~ 0.4 ± 0.8 ppb). Comparing the stack contamination filter flag for aerosol measurements (Sect. 2.2) with INP sampling periods additionally indicates no influence of stack emissions on INP filter samples. Lacking a size-selective inlet for INP sampling, it is possible that aerosols > 10 µm were present in INP samples during dust events. Surface area may be underestimated for these samples due to the $PM_{10}$ cutoff for aerosol sizing (Sect. 2.2 and S3), but we do not expect this to affect our overall conclusions as increased aerosol surface area would further reduce $n_s$ (see Results Sect. 3.3 and Discussion Sect. 4). ~~-~~

Prior to sampling, filters were cleaned by soaking in 10 % peroxide ($H_2O_2$) for 10 minutes followed by rinsing three times with deionized water, the last rinse further "polished" by passage through a 0.1 µm pore-size syringe filter (Puradisc, Whatman ®, Maidstone, U.K). Filters were pre-loaded into filter units in a laminar flow hood to further minimize contamination from handling. After

collection, each aerosol filter was placed in a 60 mm diameter sterile Petri dish (Life Science Products, Frederick, Colorado, USA) using pre-cleaned acetyl plastic forceps (Fine Science Tools, Foster City, California, USA), sealed with Parafilm and stored frozen (-20 °C). Samples were shipped in a dry shipper via Cryoport® High Vol Shipper at -180 °C and upon arrival at the laboratory were stored at -80 °C until processed, within 18 to 38 months ~~of~~ since collection. To release collected particles, filters were immersed in 5-8 mL ultrapure water (Cat. Number W4502, Sigma-Aldrich®, St. Louis, MO, USA) and shaken by hand for 20 minutes just prior to measurement. ~~Eight samples were additionally diluted 100-~~***~~fold~~*** ~~to measure INP concentrations at lower freezing temperatures (Fig. S5).~~

INP concentrations were measured using the Scripps Institution of Oceanography ~~SIO~~ Automated Ice Spectrometer (SIO-AIS), an immersion freezing droplet assay instrument that is described in detail in Beall et al. (2017). Briefly, the aerosol sample suspensions and SSW samples were distributed in 30 ×~~x~~ 50-µL aliquots into clean 96-well polypropylene sample trays (OPTIMUM® ULTRA Brand, Life Science Products). An equal number and volume of aliquots of ultrapure water accompanied each sample in the tray as a control. Trays were then inserted into an aluminum block that was cooled at -0.87 °C $min^{-1}$ until the samples ~~are~~ froze~~n~~. Cumulative INP number concentrations per temperature per volume liquid are calculated using the fraction (*f*) of unfrozen wells per given temperature interval:

$$n_{\mathrm{INP,L}} = \frac{-ln(f)}{V_d} \qquad \text{Eq. (1)}$$

where $V_d$ is the volume of the sample in each well (Vali, 1971). For aerosol filter samples, cumulative INP number concentrations are calculated using the ratio of the ultrapure water volume used for resuspension of the particles ($V_{re}$) to the volume of air sampled ($V_A$):

$$n_{\mathrm{INP}} = \frac{-ln(f)\cdot V_{re}}{V_d \cdot V_A} \qquad \text{Eq. (2)}$$

Prior to calculating $\boldsymbol{n_{INP}}$, the fraction of unfrozen wells ($f$) was adjusted for contamination in the water used for suspension by subtracting the number of frozen ultrapure water wells per temperature interval from both the total number of unfrozen wells and total wells of the sample. The $\boldsymbol{n_{INP}}$ was additionally adjusted for background INPs from filters and sampling handling processes. Background $\boldsymbol{n_{INP}}$ ~~INP concentrations~~ were estimated using measured $\boldsymbol{n_{INP}}$ ~~INP concentrations~~ in aerosol sample field blanks, which had been ~~momentarily placed~~placed in the sampling apparatus ~ 5s (without actuating the pump) before removal and unloading and storage of the filter. Seven field blank samples were collected, one every ~ 7 days of the cruise (Fig. S7). INP concentrations were measured in field blanks as described above, and the $\boldsymbol{n_{INP}}$ simulated using the mean air volume sampled (6680 L). Figure S7~~6~~ shows the estimated $\boldsymbol{n_{INP}}$ ~~$\boldsymbol{n_{INP}}$~~ across the 7 field blanks, which ranged between 1~~3~~.0 × $10^{-4}$ and ~~3.0~~7.0 × $10^{-3}$~~2~~ $L^{-1}$ at -20 °C. The freezing onset temperatures detected in the field blanks ranged between -6 and -27 °C. To correct $\boldsymbol{n_{INP}}$ ~~$\boldsymbol{n_{INP}}$~~ measured in aerosol samples for background INPs from sample handling, a linear regression ~~of the average~~ based on the geometric mean $\boldsymbol{n_{INP}}$ ~~INP concentration~~ measured in field blank suspensions ($mL^{-1}$ water) was used to estimate background concentrations of INPs in samples at all temperatures between -14.5 °C and -27 °C. The estimated background $\boldsymbol{n_{INP}}$ ~~INP concentration~~ was then subtracted from the INP concentration measured in filter sample suspension volumes in this temperature range prior to calculating $\boldsymbol{n_{INP}}$ ~~$\boldsymbol{n_{INP}}$~~. The $\boldsymbol{n_{INP}}$ ~~$\boldsymbol{n_{INP}}$~~ measured in one aerosol sample (f033) fell within the estimated INP background levels.

For this study, the detection limit was 0.68 $\boldsymbol{n_{INP}}$ ~~INPs~~ $mL^{-1}$ liquid or 0.001-0.0024 $\boldsymbol{n_{INP}}$ ~~INPs~~ $L^{-1}$ air for the ~~maximum and~~ minimum and maximum air volume sampled, respectively. To extend the upper limit of detection (i.e., the point at which all droplets have frozen) dilutions of 1:10 and 1:100 were performed on 8 samples (Fig. S8~~5~~).

The ice-active surface site density, $n_s$, is a metric used to define the ice-nucleating capabilities of an aerosol species (i.e., an aerosol sample of all the same particle type) (Kanji et al., 2017) as follows:

$$n_s = \frac{N_{ice}}{N_{tot} \times A\,(cm^2)} \qquad \text{Eq. (3)}$$

where $N_{ice}$ is the number of frozen droplets, $N_{tot}$ is the total number of particles in a monodisperse aerosol population, and $A$ is the surface area per particle.

Formatted: Font: Bold

The value of $n_s$ can also be approximated for polydisperse aerosol samples containing multiple aerosol types:

$$n_s = \frac{N_{ice}}{A_{tot}\,(cm^2)} \qquad \text{Eq. (4)}$$

where $A_{tot}$ is the total surface area of the polydisperse aerosol ~~sample~~. The difference between the $n_s$ approximation (Eq. 4) and $n_s$ (Eq. 3) is that many particle types are typically included in the $n_s$ approximation, and in an ambient aerosol measurement most of these are not IN-active~~ice nucleating~~ (see also Hiranuma et al., (2015) Sect. 2.4). Furthermore, the subset of INPs in the sample are likely also of different types, which likely have different $n_s$ in the strict sense (Eq. 3). Nevertheless, the $n_s$ approximation is a useful metric for comparing the ice-nucleating ability of different air masses and source regions and is often used for comparing data across studies of INPs measured in ambient air. It is extremely challenging to separate measurements of INPs and surface area by each particle type, and requires, for example, combining online measurements of single particle chemistry, size distributions and INPs (Cornwell et al., 2019). All $n_{\mathrm{INP}}$ and $n_s$ are reported normalized to a standard temperature of 273.15 °K and pressure of 1013 hPa.

Heat and ~~hydrogen~~ peroxide ~~-~~treatments were applied to a subset of samples (12 of 26) to test for heat-labile biological (e.g., proteinaceous) and organic INP composition, respectively, following the procedure described in ~~(~~McCluskey et al.~~,~~ (2018b) and~~;~~ Suski et al.~~,~~ (2018). The 12 samples were selected based on sampling location with the aim of getting a representative measurement from each region. For each heat-treated sample, a 2 mL aliquot of the original ultrapure water suspension was heated to 95 °C for 20 min in a water bath and re-tested ~~to assess the reduction in INP concentrations~~for changes in $\boldsymbol{n_{\mathrm{INP}}}$. For peroxide treatments, 1.6 mL of the original suspension was combined with 0.8 mL of 30% ~~$H_2O_2$~~ peroxide (Sigma Aldrich®, St. Louis, Missouri, USA) to achieve a final concentration of 10%, then the mixture was ~~immersed in water, and~~ heated to 95 °C for 20 min while being illuminated with two 26-W UVB fluorescent bulbs ~~to generate hydroxyl radicals~~. To remove residual ~~$H_2O_2$~~ peroxide and~~, to~~ prevent ~~otherwise significant~~ freezing point depression, the solution was cooled and catalase (Cat. Number IC10042910, MP Biomedicals, Santa Ana, California, USA) was added~~. Since catalase is itself decomposed by $H_2O_2$, while simultaneously catalyzing peroxide's disproportionation into water and oxygen, the enzyme was added in several 20 µL aliquots, allowing several minutes between each, until no effervescence resulted upon its addition.~~ Figure S7 shows the estimated $n_{\mathrm{INP}}$ in a heat and peroxide-treated blank

sample. Fisher's Exact Test was applied to frozen and unfrozen well fractions between each untreated sample and its corresponding treated sample to test for significant differences ($p < 0.05$). Note that significant difference in frozen well fraction is insufficient as a sole indicator of sensitivity in peroxide treated samples because samples are diluted 2:3 (by 33%) compared to untreated samples. As $n_{INP}$ ~~INP concentrations~~ can be corrected for the dilution by scaling (as opposed to frozen well fractions), the overlap in 95% binomial sampling confidence intervals (Agresti and Coull, 1998) between the untreated and peroxide-treated sample is an additional indicator of sensitivity for a given data point in the peroxide-treated sample spectrum within ± 0.2 °C, the uncertainty in the SIO-AIS temperature measurement (Beall et al., 2021). A lack of overlap in the 95% binomial sampling confidence interval within ± 0.2 °C equates to a significance threshold of $p < 0.005$ (Krzywinski and Altman, 2013).

INP concentrations were additionally measured in in untreated, heat-treated, and peroxide-treated subsamples from an archived suspension of the soil dust sample N12 SD for comparison with this study (DeMott et al., 2018; hereafter referred to as "N12-SD"). N12 SD (sample CD1 in Megahed 2007) is sedimented airborne dust that was carried in boundary layer winds north and then east from the desert in central Egypt during a sandstorm to a sampling point ~50 km north of Cairo, collected on 18th Feb 2003. The sample was stored in a "clean bottle" (no temperature of storage given) for further analysis (Megahed 2007). Briefly, the sample was generated during the recent laboratory intercomparison of INP measurements (DeMott et al., (2018), collected on a 0.2 µm Nuclepore polycarbonate membrane filter (Whatman ®, Chicago, Illinois, USA) and stored frozen at -20 °C until processed, as described in DeMott et al (2018).

Formatted: Font: (Default) Times New Roman

## 2.5 INP Measurements in SSW

Formatted: Font: Bold

Formatted: Font: Bold

Formatted: Font: Bold

INP concentrations were additionally measured in 10 SSW samples. For seawater sampling, a water intake vertical steel pipe was positioned on the starboard of the ship approximately 2 m below the sea surface level. The seawater was pumped into a 200 L stainless steel tank and continuously exchanged at a rate of 3000 L $h^{-1}$. SSW samples for INP analysis were collected in 15 mL sterile centrifuge tubes (Falcon™, ThermoFisher Scientific, Waltham, Massachusetts, USA) and stored frozen at -20 °C until they could be shipped in a dry shipper via Cryoport® (-180 °C) and ultimately stored at -80 °C as for aerosol samples until processed as described above (Sect.

2.4), within 18 to 38 months since collection. Storage duration was not correlated with INP concentration changes in frozen marine and coastal precipitation samples (Beall et al., 2020). Heat and hydrogen peroxide treatments as described above were applied to five 5 SSW samples from the Arabian Sea and the Gulf of Aden. The focus on these regions was motivated by the detection of marine aerosol originating from the upwelling region in Somalia reported in (Edtbauer et al., (2020; see Sect. 3.3).of these. To assess the contribution of submicron INPs to total measured INPs, 2 mL of SSW was filtered through a 0.2 µm sterile syringe-filter (Acrodisc® Pall®, Port Washington, New York, USA) and re-tested.

INP concentrations in SSW collected at the Ellen Browning Scripps Memorial Pier at Scripps Institution of Oceanography (SIO; 32.8662 N, 117.2544 W) were assessed in 17 samples for comparison with SSW collected during AQABA. Samples were collected between 31 Jan and 7 May 2016 in 15-30 mL sterile centrifuge tubes (Falcon™, ThermoFisher Scientific, Waltham, Massachusetts, USA) at depths of 1-3m and processed immediately using the SIO-AIS as described above.

**2.5 FLEXPART Back Trajectories**

Air mass 72-hour back-trajectories for each sample were simulated using the FLEXible PARTicle dispersion model (FLEXPART) in backward mode (Stohl et al., 1998). NOAA Climate Forecast System (CFS) short-duration (t < 6 h) forecasts (Saha et al., 2014) were used as three-dimensional forcing datasets. Particle releases from 35 m above sea level (ASL) followed the vessel track using vessel position information from the European Common Automatic Weather Station (EUCAWS; http://eumetnet.eu/; last access Sept. 2021).

# 3 Results and Discussion

## 3.1 Characteristics of INPs Observed During AQABA

## 3.1 Characteristics of INP INP Concentrations s Observed in Aerosol During AQABA

A total of 26 aerosol samples were collected in July – August 2017 during AQABA for offline measurements of INPs. The INP concentrations ($n_{INP}$) measured in samples collected in the

Formatted: Font: Not Italic

Mediterranean Sea, the Red Sea, the Gulf of Aden, Arabian Sea, Gulf of Oman, and Arabian Gulf spanned up to 2~~3~~ orders of magnitude at -15 °C (Fig. 1, Table 1), between $5 \times 10^{-3}$ and $5 \times 10^{-1}$ $L^{-1}$. This range agrees within an order of magnitude with that of ~~(~~Prodi et al.~~,~~ (1983) who measured $n_{INP}$ in the Mediterranean, Red Sea, Gulf of Aden and Indian Ocean nearly 4 decades prior to the present study ($4 \times 10^{-2}$ to 2 $L^{-1}$ at -16 °C). Average ambient dust concentrations during each sampling period ranged from 2-490 µg $m^{-3}$ ($PM_{10}$ Table 1). There is no agreed-upon standard for definition of extreme dust events in the literature, though the 24-hr average WHO or US EPA health standards for average $PM_{10}$ are commonly used (Gandham et al., 2020; Khaniabadi et al., 2017). Using the US EPA health standard for $PM_{10}$ as a threshold for extreme events (150 µg $m^{-3}$), 14 of the 26 samples were collected during dust events. This is conservative given the equivalent WHO guideline for $PM_{10}$ is 50 µg $m^{-3}$ (WHO, 2005), in which case 22 of the 26 sampling periods would be classified as dust events. Prior studies have reported comparable $PM_{10}$ levels during dust events in the region (Gandham et al., 2020; Krasnov et al., 2016; Shahsavani et al., 2012).

Figs. S9-S10 show the extent of k-means clustered FLEXPART back-trajectories below the altitude of 1500 m (see Sect. S5 for details). This threshold was applied to eliminate most of the free tropospheric parts of the back-trajectories and was selected based on the MERRA-2 monthly average planetary boundary layer (PBL) heights during the campaign period, which were 200-700 m over the ocean and up to 1700 m over land. ~~FLEXPART 72 hour~~ A~~a~~ir mass back trajectories show that source regions included the Mediterranean, Nile Delta, Sinai Peninsula (f006-f008, f038), Northeast Egypt (f009-f010), Iran (f023-f024), and Southern and Eastern Europe (f040, f042, f044) (S9-S16). M~~m~~any ~~of~~ samples collected during extreme dust events (f013, f014, f016, f018, and f020) were influenced by emissions from North Africa and the Arabian Peninsula (Figs S9~~8~~-S10~~9~~, S12-14). ~~Other source regions included the Mediterranean, Nile Delta, Sinai Peninsula (f006-f008), Northeast Egypt (f009-f010), Iran (f024), and Southern and Eastern Europe (f040, f042, f044)~~. The ranges of aerosol surface area concentrations for all sampling periods were < 320 $\mu m^2$ $cm^{-3}$, with the exception of f024, for which aerosol surface area range was > 600 $\mu m^2$ $cm^{-3}$ (Table 1).

Formatted: Font: Not Bold
Formatted: Font: Not Bold
Formatted: Font: Not Bold
Formatted: Font: Not Bold
Formatted: Superscript
Formatted: Not Superscript/ Subscript
Formatted: Font: Not Bold

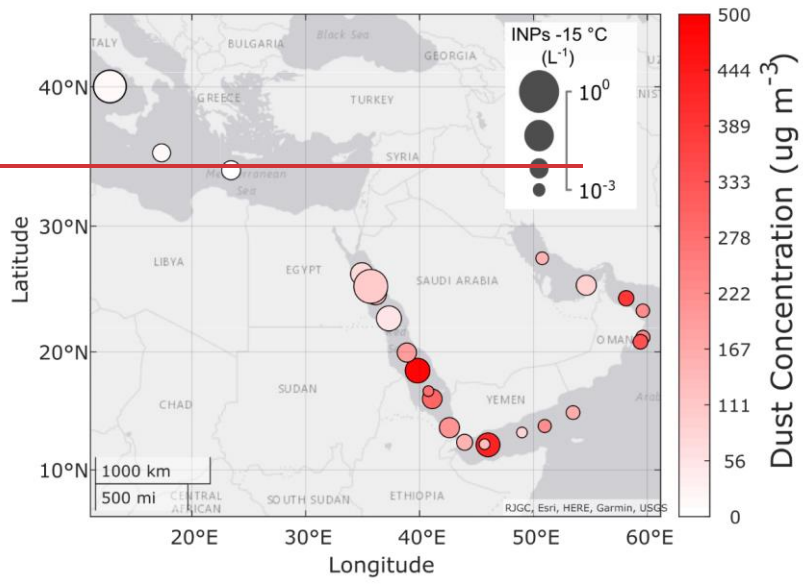
INPs -15 °C
(L-1)
10^0
10^-3
Dust Concentration (ug m-3)
500
444
389
333
278
222
167
111
56
0
Latitude
40°N
30°N
20°N
10°N
Longitude
20°E
30°E
40°E
50°E
60°E
1000 km
500 mi
RJGC, Esri, HERE, Garmin, USGS
TURKEY
SYRIA
LIBYA
EGYPT
SAUDI ARABIA
SUDAN
CHAD
YEMEN
ETHIOPIA
SOUTH SUDAN
GREECE
GEORGIA
BULGARIA

466

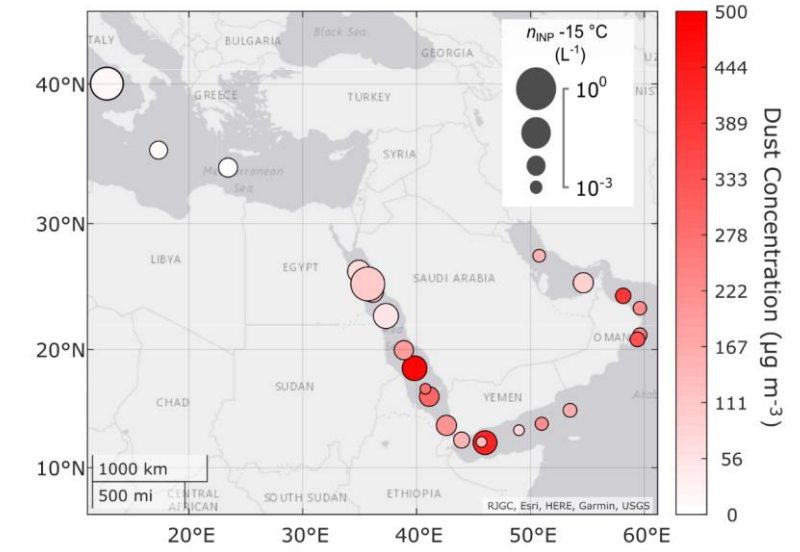
nINP -15 °C
(L-1)
10^0
10^-3
Dust Concentration (µg m-3)
500
444
389
333
278
222
167
111
56
0
40°N
30°N
20°N
10°N
20°E
30°E
40°E
50°E
60°E
1000 km
500 mi
RJGC, Esri, HERE, Garmin, USGS
TURKEY
SYRIA
LIBYA
EGYPT
SAUDI ARABIA
SUDAN
CHAD
YEMEN
ETHIOPIA
SOUTH SUDAN
GREECE
GEORGIA
BULGARIA

467

**Figure 1.** Map of the sample locations for 26 aerosol samples collected on the RV *Kommandor Iona* during Air Quality and climate change in the Arabian BAsin (AQABA; see also Figs. S1-S2 and S9-S10). Measured $n_{INP}$ ~~INP concentrations~~ spanned ~~three~~ 2 orders of magnitude at -15 °C, from $5 \times 10^{-3}$ to $5 \times 10^{-1}$ ~~0.5~~ $L^{-1}$. Marker sizes indicate abundance of INPs. Marker colors indicate the average ambient dust mass concentration during the sampling period from hourly MERRA-2 reanalysis data.

**Table 1.** Summary of aerosol samples collected during AQABA. "—" indicates where data are missing; "NaN" indicates values below detection limit. Locations are given at the transect midpoint during each sampling period.

| Sample ID | Start datetime (UTC) | Stop datetime (UTC) | Latitude (° N) | Longitude (° E) | $n_{INP}$ 15 °C ($L^{-1}$) | Sample Volume (L air) | Average Aerosol Surface Area ($PM_{10}$, $\mu m^2$ $cm^{-3}$) | Aerosol Surface Area [min, max] ($PM_{10}$, $\mu m^2$ $cm^{-3}$) | Average Dust Concentration ($PM_{10}$, $\mu g$ $m^{-3}$) | Average Seasalt ($PM_{10}$, $\mu g$ $m^{-3}$) |
|---|---|---|---|---|---|---|---|---|---|---|
| f006 | 05-Jul 05:46 | 05-Jul 11:37 | 26.224 | 35.025 | 0.0146 | 3370 | 290 | [199, 375] | 170 | - |
| f007 | 05-Jul 16:40 | 05-Jul 19:51 | 26.291 | 34.933 | 0.0475 | 2588 | 260 | [222, 289] | 70 | - |
| f008 | 06-Jul 07:09 | 06-Jul 14:08 | 25.225 | 35.775 | 0.1161 | 5225 | 177 | [106, 259] | 100 | - |
| f009 | 07-Jul 05:50 | 07-Jul 15:07 | 25.011 | 35.947 | 0.0838 | 6940 | 352 | [253,416] | 110 | - |
| f010 | 08-Jul 16:33 | 09-Jul 05:59 | 23.623 | 36.931 | 0.0592 | 8073 | 219 | [163, 287] | 50 | - |
| f013 | 14-Jul 12:26 | 14-Jul 16:13 | 18.687 | 39.672 | 0.0585 | 2283 | 264 | [176, 352] | 490 | 10 |
| f014 | 15-Jul 05:10 | 15-Jul 11:49 | 16.552 | 40.834 | 0.0348 | 4000 | 271 | [204, 343] | 300 | 5 |
| f016 | 18-Jul 07:04 | 18-Jul 14:52 | 11.939 | 45.334 | 0.0534 | 4690 | 265 | [158, 391] | 430 | - |
| f018 | 22-Jul 10:20 | 22-Jul 18:44 | 20.941 | 59.474 | 0.0166 | 5025 | 212 | [171, 238] | 340 | - |
| f019 | 23-Jul 04:48 | 23-Jul 13:34 | 21.410 | 59.691 | 0.0145 | 5270 | 218 | [190, 240] | 240 | - |
| f020 | 25-Jul 17:15 | 26-Jul 04:02 | 23.976 | 58.809 | 0.0184 | 6511 | - | - | 390 | 5 |
| f023 | 04-Aug 04:05 | 04-Aug 11:56 | 28.084 | 50.284 | 0.0112 | 4720 | 835 | [756, 965] | 150 | 4 |
| f024 | 05-Aug 05:57 | 05-Aug 13:53 | 25.432 | 53.853 | 0.0371 | 5221 | 357 | [206, 827] | 90 | - |
| f025 | 07-Aug 09:26 | 07-Aug 16:46 | 23.814 | 59.186 | 0.0129 | 4410 | 55 | [46, 72] | 220 | 12 |
| f030 | 13-Aug 07:08 | 14-Aug 11:06 | 15.970 | 54.705 | 0.0132 | 15111 | 28 | [16, 144] | 160 | - |
| f031 | 14-Aug 15:03 | 15-Aug 09:03 | 14.003 | 52.357 | 0.0121 | 12972 | 25 | [19, 105] | 230 | - |
| f032 | 15-Aug 09:42 | 15-Aug 15:07 | 13.354 | 49.432 | 0.0059 | 3260 | 96 | [82, 147] | 80 | 6 |
| f033 | 16-Aug 09:30 | 16-Aug 13:17 | 12.208 | 45.706 | NaN | 2280 | 73 | [51, 135] | 130 | 2 |

Formatted: Font: 12 pt
Formatted: Justified
Formatted Table

| | | | | | | | | | | |
|---|---|---|---|---|---|---|---|---|---|---|
| f034 | 16-Aug 13:27 | 17-Aug 07:04 | 12.177 | 45.429 | 0.0206 | 8464 | 168 | [51, 372] | 150 | 1 |
| f035 | 17-Aug 07:30 | 17-Aug 14:55 | 13.308 | 42.974 | 0.0365 | 4460 | 340 | [244, 409] | 210 | 2 |
| f036 | 18-Aug 06:36 | 18-Aug 15:03 | 16.290 | 41.038 | 0.0057 | 6634 | 208 | [160, 428] | 280 | 2 |
| f037 | 19-Aug 07:05 | 20-Aug 07:04 | 18.699 | 39.609 | 0.0326 | 18806 | 240 | [175, 331] | 190 | 7 |
| f038 | 21-Aug 07:22 | 21-Aug 16:01 | 24.112 | 36.554 | 0.0422 | 6700 | 256 | [202, 295] | 150 | - |
| f040 | 26-Aug 16:02 | 27-Aug 07:04 | 33.803 | 24.814 | 0.0314 | 9030 | 90 | [58, 142] | < 10 | 3 |
| f042 | 28-Aug 07:51 | 28-Aug 16:02 | 35.310 | 17.965 | 0.0279 | 6396 | 163 | [131, 222] | < 10 | 2 |
| f044 | 31-Aug 08:30 | 31-Aug 20:16 | 39.569 | 13.380 | 0.4572 | 11296 | 211 | [148, 255] | < 10 | - |

| Sample ID | Start datetime (UTC) | Stop datetime (UTC) | Latitude | Longitude | | Sample Volume (L air) | Aerosol Surface Area ($\mu m^2$ $cm^{-3}$) | Average Dust Concentration ($\mu g\ m^{-3}$) | Average Seasalt Concentration ($\mu g\ m^{-3}$) |
|---|---|---|---|---|---|---|---|---|---|
| | | | | | 0.0146 | | | | |
| f006unt | 05-Jul 05:46 | 05-Jul 11:37 | 26.224 | 35.025 | 0.0475 | 3370 | 290 | 170 | |
| f007unt | 05-Jul 16:40 | 05-Jul 19:51 | 26.291 | 34.933 | 0.1161 | 2588 | 260 | 70 | |
| f008unt | 06-Jul 07:09 | 06-Jul 14:08 | 25.225 | 35.775 | 0.0838 | 5225 | 180 | 100 | |
| f009unt | 07-Jul 05:50 | 07-Jul 15:07 | 25.011 | 35.947 | 0.0592 | 6940 | 350 | 110 | |
| f010unt | 08-Jul 16:33 | 09-Jul 05:59 | 23.623 | 36.931 | 0.0585 | 8073 | 220 | 50 | |
| f013unt | 14-Jul 12:26 | 14-Jul 16:13 | 18.687 | 39.672 | 0.0348 | 2283 | 260 | 490 | |
| f014unt | 15-Jul 05:10 | 15-Jul 11:49 | 16.552 | 40.834 | 0.0534 | 4000 | 270 | 300 | |
| f016unt | 18-Jul 07:04 | 18-Jul 14:52 | 11.939 | 45.334 | 0.0166 | 4690 | 260 | 430 | |
| f018unt | 22-Jul 10:20 | 22-Jul 18:44 | 20.941 | 59.474 | 0.0145 | 5025 | 210 | 340 | |
| f019unt | 23-Jul 04:48 | 23-Jul 13:34 | 21.410 | 59.691 | 0.0184 | 5270 | 220 | 230 | |
| f020unt | 25-Jul 17:15 | 26-Jul 04:02 | 23.976 | 58.809 | 0.0112 | 6511 | - | 390 | |
| f023unt | 04-Aug 04:05 | 04-Aug 11:56 | 28.084 | 50.284 | 0.0371 | 4720 | 830 | 150 | |
| f024unt | 05-Aug 05:57 | 05-Aug 13:53 | 25.432 | 53.853 | 0.0129 | 5221 | 360 | 90 | |
| f025unt | 07-Aug 09:26 | 07-Aug 16:46 | 23.814 | 59.186 | 0.0132 | 4410 | 50 | 220 | |
| f030unt | 13-Aug 07:08 | 14-Aug 11:06 | 15.970 | 54.705 | 0.0121 | 15111 | 30 | 160 | |
| f031unt | 14-Aug 15:03 | 15-Aug 09:03 | 14.003 | 52.357 | 0.0059 | 12972 | 30 | 220 | |

Formatted: Font: (Default) Times New Roman, 8 pt

| | | | | | | | | |
|---|---|---|---|---|---|---|---|---|
| | 15 Aug | 15 Aug | | | | | | |
| f032unt | 09:42 | 15:07 | 13.354 | 49.432 | NaN | 3260 | 100 | 80 |
| | 16 Aug | 16 Aug | | | | | | |
| f033unt | 09:30 | 13:17 | 12.208 | 45.706 | 0.0206 | 2280 | 90 | 130 |
| | 16 Aug | 17 Aug | | | | | | |
| f034unt | 13:27 | 07:04 | 12.177 | 45.429 | 0.0365 | 8464 | 170 | 150 |
| | 17 Aug | 17 Aug | | | | | | |
| f035unt | 07:30 | 14:55 | 13.308 | 42.974 | 0.0057 | 4460 | 340 | 210 |
| | 18 Aug | 18 Aug | | | | | | |
| f036unt | 06:36 | 15:03 | 16.290 | 41.038 | 0.0326 | 6634 | 210 | 280 |
| | 19 Aug | 20 Aug | | | | | | |
| f037unt | 07:05 | 07:04 | 18.699 | 39.609 | 0.0422 | 18806 | 240 | 190 |
| | 21 Aug | 21 Aug | | | | | | |
| f038unt | 07:22 | 16:01 | 24.112 | 36.554 | 0.0314 | 6700 | 260 | 140 |
| | 26 Aug | 27 Aug | | | | | | |
| f040unt | 16:02 | 07:04 | 33.803 | 24.814 | 0.0279 | 9030 | 90 | <10 |
| | 28 Aug | 28 Aug | | | | | | |
| f042unt | 07:51 | 16:02 | 35.310 | 17.965 | 0.4572 | 6396 | 160 | 10 |
| | 31 Aug | 31 Aug | | | | | | |
| f044unt | 08:30 | 20:16 | 39.569 | 13.380 | $n_{INP}$ -15 °C ($L^{-1}$) | 11296 | 210 | 10 |

Formatted: Font: (Default) Times New Roman, 8 pt

## 3.2 Seawater Source Potential

The $n_{INP}$ values in 10 SSW samples collected during AQABA were used to characterize the INP source potential of SSA generated by bubble bursting (Wang et al., 2017). Results from prior studies have demonstrated that jet droplets are a more efficient transfer vehicle than film drops of INPs into SSA particles (Mitts et al., 2021; Wang et al., 2017). We measured the $\boldsymbol{n_{INP}}$ in SSW to test whether the seawater source strength was comparable to that of prior studies, or whether the SSW was possibly enriched with INPs due to biological activity or even dust deposition (Cornwell et al., 2020).

Formatted: Font: Not Italic

Figure S17 shows how the $n_{INP}$ measured at -19 °C in 10 seawater samples varied by the sample collection location. Concentrations ranged between 1 and 50 $\boldsymbol{n_{INP}}$ $mL^{-1}$ and were highest between the Gulf of Oman and the Gulf of Aden. This region exhibited relatively high chlorophyll *a* during the cruise, with levels between 1 and 30 mg $m^{-3}$ (Fig. S18). In Fig. 2, $\boldsymbol{n_{INP}}$ were compared with SSW from the Ellen Browning Scripps Memorial Pier in coastal Southern California (SIO Pier),

Cabo Verde in the Northeast Atlantic, the Southern Ocean (McCluskey et al., 2017), and the Northwest Atlantic (Schnell, 1977). AQABA $\boldsymbol{n_{INP}}$ were most comparable with Gong et al.'s (2020) observations in Cabo Verde. The lack of any unusually high INP spectra suggests that INP enrichment due to dust deposition (Cornwell et al. 2020) was absent or infrequent. It is possible that storage of SSW samples (Sect. 2.5) could have decreased measured $\boldsymbol{n_{INP}}$, though we expect

that $n_{INP}$ would be decreased by no more than 10× in untreated samples stored frozen (see discussion below).

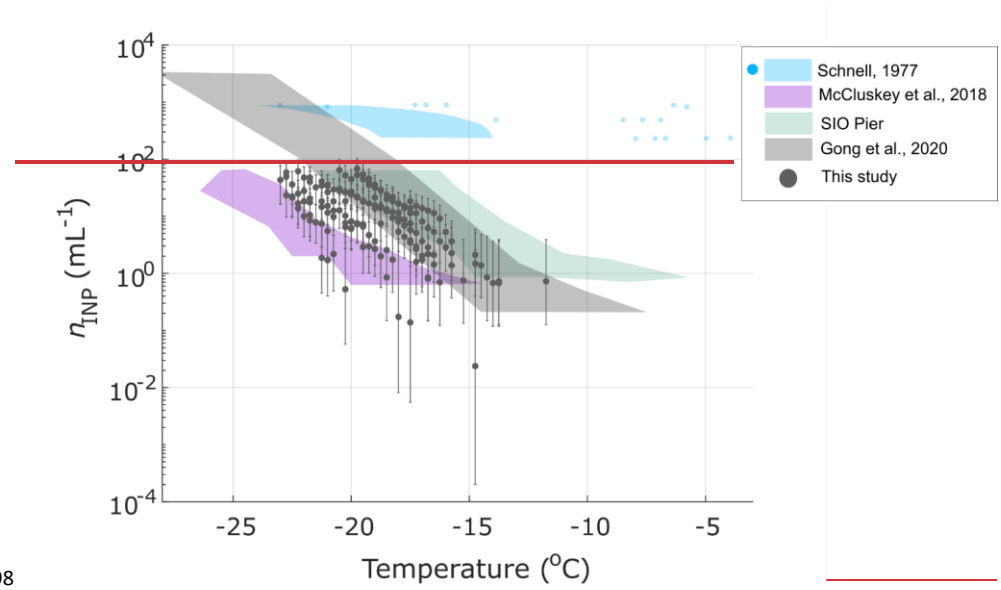

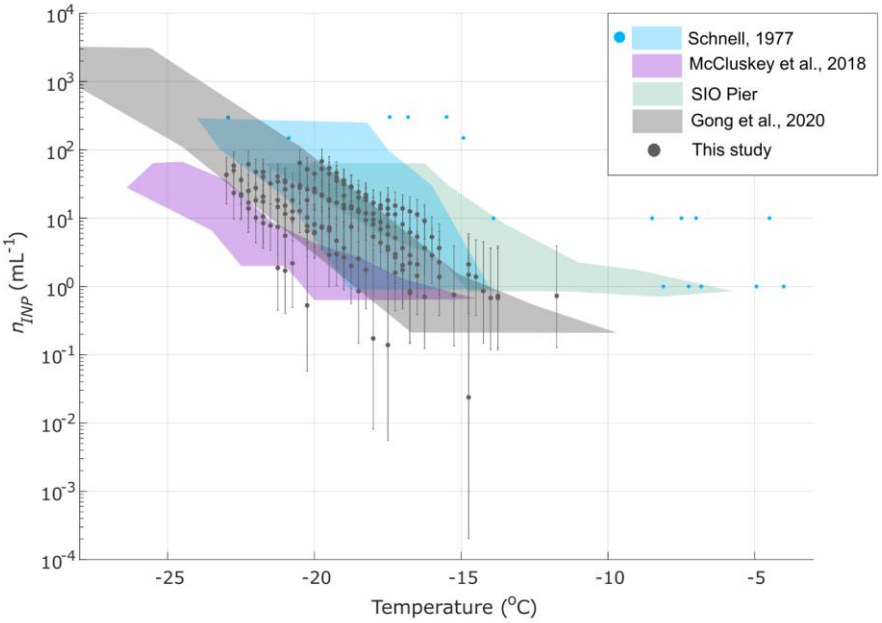


**Figure 2.** Measured $n_{INP}$ in 10 SSW samples collected during AQABA. Also shown are the composite INP spectrum of 14 coastal SSW samples collected on São Vincente Island, Cabo Verde (Gong et al., 2020), 17 coastal SSW samples collected at the Ellen Browning Scripps Pier (green shading), and 12 SSW samples collected in the Southern Ocean (McCluskey et al., 2018d). Schnell's (1977) SSW measurements are represented as a composite spectrum of 24 samples (blue shaded region) and 5 additional spectra (blue markers) from samples that exhibited higher freezing temperatures. All spectra presented are uncorrected for freezing point depression.

Offline treatments for testing heat lability, organic composition, and size were applied to 5 of the 10 seawater samples (Methods Sec. 2.5). Heat and 0.2 μm filtering treatments suggest that a large fraction of the seawater INPs were heat sensitive and larger than 0.2 μm (Fig. S19). These results are indicative of the POC type of marine INP defined in McCluskey et al. (2018a), though this result should be interpreted with caution as storage could potentially have increased sensitivity to filtering treatments.

**Formatted:** Font: (Default) Times New Roman, 12 pt

**Formatted:** Normal

**Formatted:** Font: (Default) Times New Roman, 12 pt

**Formatted:** Font: (Default) Times New Roman, 12 pt, Bold

**Formatted:** Font: (Default) Times New Roman, 12 pt

**Formatted:** Font: (Default) Times New Roman, 12 pt

**Formatted:** Font: Bold

Understanding of storage impacts on INPs measured in SSW is lacking. However, Beall et al., (2020) showed that average INP concentration changes for untreated coastal precipitation samples due to frozen storage were within 2× of $n_{INP}$ measured in fresh samples, with changes at the upper or lower end of the 95% CI exceeding 10× for some freezing temperatures. If SSW samples are similarly sensitive to storage, we would expect INP concentration changes to be within 2× on average, but up to > 10× for any particular untreated sample. Beall et al. (2020) also reported similar changes INPs < 0.45 µm with a greater tendency toward losses, which indicates that storage may have caused increased sensitivity to the filter treatments applied to stored samples.

### 3.3 Ice-active Surface Site Densities in Aerosol

In Fig. ~~ure~~ ~~3~~2, approximated ice ~~nucleation~~ -active surface site densities ($n_s$) in aerosol samples are compared with multiple population-specific observations and parameterizations for dust and marine INPs. The AQABA measurements are also compared with observations from dust-laden air over the Tropical Atlantic (Price et al., 2018). Overall, observations nearly bridge the full regime between the M18 parameterization for marine INPs (~~hereafter "M18";~~ McCluskey et al., 2018c), and multiple dust INP parameterizations based on laboratory studies of surface dust. At higher temperatures, between -5 and -12 °C, most observations show agreement with the composite spectrum of $n_s$ observed in a range of marine and coastal environments from DeMott et al. (2016) and ~~(~~Yang et al.~~,~~ (2020)~~Yang et al. (2019)~~, and/or the ~~Atkinson et al. (2013)~~A13 K-feldspar parameterization. Between -10 and -20 °C, several samples agree with the M18 marine INP parameterization within an order of magnitude, whereas two to three $n_s$ spectra approach the U17 and N12 laboratory-derived dust INP parameterizations within an order of magnitude (Niemand et al., 2012; Ullrich et al., 2017), depending on temperature. Multiple samples (~8) additionally agreed with Price et al.'s (2018) observations of INPs between 30-3500 m above the dust-laden~~y~~ Tropical Atlantic, and most agree with the Gong et al. (2020) surface-level observations, measured at Cabo Verde in the same region as Price et al. (2018) ~~(Cabo Verde)~~.

Formatted: Justified

Formatted: Font: Bold

Formatted: Font: Bold

Formatted: Font: Bold

Formatted: Font: Bold

Formatted: Font: Bold

Formatted: Font: Bold

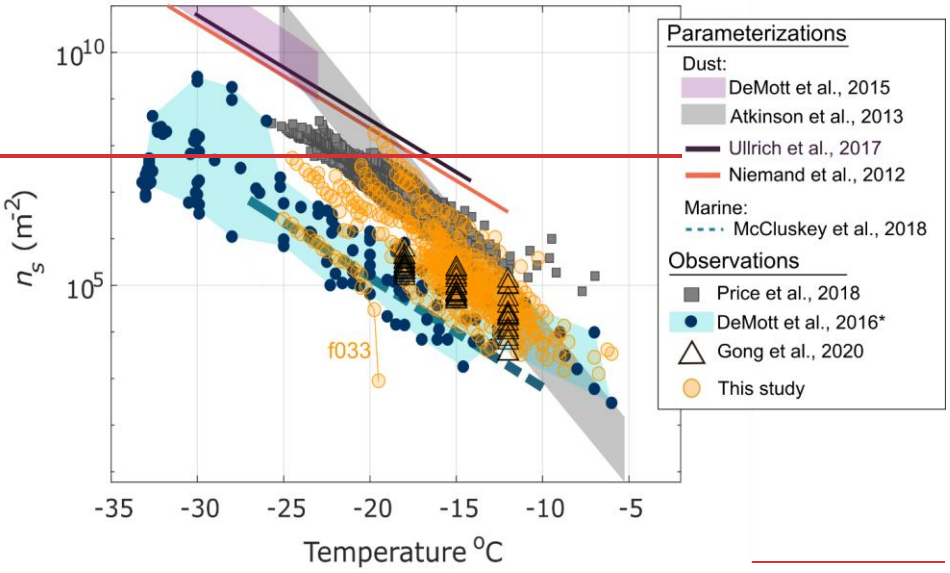
Parameterizations
Dust:
DeMott et al., 2015
Atkinson et al., 2013
Ullrich et al., 2017
Niemand et al., 2012
Marine:
McCluskey et al., 2018
Observations
Price et al., 2018
DeMott et al., 2016*
Gong et al., 2020
This study
f033
$10^{10}$
$10^{5}$
$n_s$ ($m^{-2}$)
-35 -30 -25 -20 -15 -10 -5
Temperature °C

538

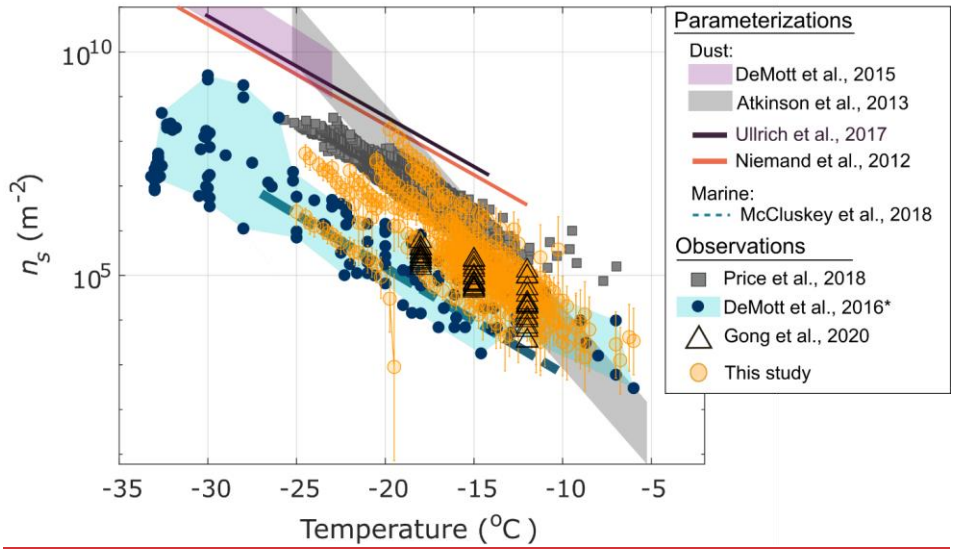
Parameterizations
Dust:
DeMott et al., 2015
Atkinson et al., 2013
Ullrich et al., 2017
Niemand et al., 2012
Marine:
McCluskey et al., 2018
Observations
Price et al., 2018
DeMott et al., 2016*
Gong et al., 2020
This study
$10^{10}$
$10^{5}$
$n_s$ ($m^{-2}$)
-35 -30 -25 -20 -15 -10 -5
Temperature (°C)

539

**Figure 32.** Ice-active surface-nucleation site densities ($n_s$) as a function of temperature for 25 of 26 aerosol samples collected during AQABA. Gong et al. (2020) and Price et al. (2018) measured INPs in dust-dominant air masses in the tropical east Atlantic, with minor contributions from SSA, while the DeMott et al. (2016) measurements were collected across a range of locations and conditions within the marine boundary layer comprising air masses mostly dominated by relatively pristine marine SSA. INP concentrations measured in sample f033 were below the detection limits imposed by field blanks (see Sect. 2.4, Fig. S76). Error bars represent 95% binomial sampling confidence intervals (Agresti and Coull, 1998). Sample f020 is not shown due to missing aerosol surface area data during the sampling period. For the 8 samples on which a dilution was performed (Fig. S8), $n_s$ for both the raw undiluted and diluted sample are shown. *DeMott et al. (2016) data shown have been updated with additional data from Yang et al. (2020).

Considering the frequency of dust events encountered (dust concentration > 150 µg $m^{-3}$, see Table 1), and the high probability that dust was the dominant aerosol source during most sampling periods, it is striking that most $n_s$ spectra observed are 1-3 orders of magnitude lower than the values predicted by dust parameterizations. As noted in Gong et al. (2020), some deviations could be expected due to the difference between approximated $n_s$ based on total particle surface area in ambient measurements and true $n_s$ based on surface area of a homogeneous aerosol population (see Methods Sect. 2.4). ~~The FLEXPART back trajectories show that air masses for multiple samples originated from densely populated regions such as Southern and Eastern Europe (f040, f042, f044, Fig S9). The back trajectories also show that for samples f006-f008, f010, and f038, air masses were influenced by the populous region around the Nile River Delta. Agricultural soil dusts represent a potential constituent of the INPs observed from these regions~~. ~~A range of $n_s$ has been reported in studies of agricultural soil dusts, the lower end of which agrees with the $n_s$ observed in the present study between -8 and -25 °C (Steinke et al., 2016; Tobo et al., 2014; O'Sullivan et al., 2014).~~

Given the marine environment in which sampling ~~occurred~~took place, a significant amount of sea spray aerosol (SSA) was also detected in many of the sampled airmasses, using sea salt as a proxy (Table 1), and likely present in others for which no composition data were available. Edtbauer et al. (2020) reported the detection of high levels of dimethyl sulfide (DMS, up to 800 ppt) in the

Formatted: Justified

Formatted: Superscript

Formatted: Justified

Gulf of Aden associated with a local phytoplankton bloom during AQABA (as evidenced by visible bioluminescence around the ship at night) as well as high levels of dimethyl sulfone ($DMSO_2$) and other marine biogenic volatile organic carbons (VOCs) from the Somalian upwelling region. As mentioned above, the $n_s$ for most samples between -6 and -18 °C agree with $n_s$ derived from observations across various locations within the marine boundary layer (Fig. 32). However, considering that SSA is associated with 1000 times fewer IN sites per unit surface area than dust (i.e. 1000× lower $n_s$) (McCluskey et al., 2018c), the characteristically low IN activity of untreated SSW (even in light of the modest changes expected from storage, Sect. 3.2), and the frequency of dust events during AQABA, our findings suggest it is unlikely that the observed INPs originated from SSA. ~~and the high relative abundance of dust compared to sea salt concentrations (Table 1), it is unlikely that the observed INPs originated from SSA~~. In general, detection of marine INPs in ambient aerosol is challenging due to their low relative abundance and decreased efficiency compared to dust (DeMott et al., 2016; McCluskey et al., 2018c). Thus, while SSA contributed to the measured aerosol surface area (Table 1), it is unlikely that the INPs observed in this study were marine in origin, or at least that this is indiscernible in the present study or based on present parameterizations of these populations.

Heterogeneous aerosol composition in the sampled air masses likely contributed to some of the low $n_s$ spectra observed due to the contribution of non-INPs to the measured aerosol surface area (see description of $n_s$ approximation in Sect. 2.4). However, the difference between $n_s$ observed during the most extreme dust events, i.e., when the aerosol population was likely approaching homogeneity in composition, and the $n_s$ predicted from N12 and U17 was still greater than 2 orders of magnitude. Figures 43(a) and (b) show overlap in $n_{INP}$ and $n_s$ observed in samples collected in low dust and high dust conditions, indicating that the INP populations observed during AQABA exhibited similar ~~efficiencies~~ IN activity despite variation in total aerosol composition and dust loading. No correlation was found between $n_{INP}$ and aerosol surface area (Fig. S207), $PM_{10}$ or dust concentration. This result is in contrast to Price et al. (2018) who found the variability in $n_{INP}$ to be largely determined by variability in dust loading or aerosol surface area. ~~(~~Price et al.~~,~~ (2018) reported higher maximum aerosol surface area concentrations of ~1500 µm $cm^{-3}$ from three samples collected in an exceptionally optically thick layer, compared to the maximum of 965 µm $cm^{-3}$ in the present study (Table 1). Yet overall, the aerosol surface area concentrations compare very well with those observed by (Price et al., 2018), indicative of comparable dustiness in the two

Formatted: Not Superscript/ Subscript

Formatted: Font: Not Italic

Formatted: Font: Not Italic

Formatted: Subscript

Formatted: Font: Not Italic

Formatted: Superscript

studies. Excluding the ~~three~~case mentioned above ~~samples, Price et al. (2018) collected in an exceptionally optically thick dust layer~~, the average aerosol surface area was 227 ± 68 µm$^2$ cm$^{-3}$ vs. 226 ± 26 µm$^2$ cm$^{-3}$ for the present study. Furthermore, the sample with the highest $n_s$ at -15 °C (f04~~0~~) was collected when dust concentrations were lowest (< 10~~2~~ µg m$^{-3}$) (Fig. ~~3~~, Table 1). This is also in direct contrast to Price et al. (2018), who found that the highest $n_s$ observed corresponded to the highest dust loading.

~~Gong et al. (2020) also observed $n_s$ lower by more than 2 orders of magnitude compared to N12 and U17 despite the large fraction of supermicron INPs (77-83% depending on temperature), and that the supermicron particles were mainly mineral dust. The large differences between parameterized $n_s$ for dust, and $n_s$ observed in both Gong et al. (2020) and the present study between -12 and -25 °C demonstrate that existing $n_s$ based parameterizations may not faithfully represent $n_s$ at moderate freezing temperatures, despite proximity to major source regions. Whereas DeMott et al. (2015a) found that for temperatures < -20 °C, mineral dust particles from Saharan and Asian deserts may be parameterized as a common particle type, our findings suggest that characteristic $n_s$ parameterizations for dust from different source regions may be needed > -20 °C, or, alternatively, that this temperature regime requires an alternative to an $n_s$ based parameterizations. Gong et al. (2019a) demonstrated that predicting $n_{INP}$ from surface area size distributions alone may not be feasible in environments where the aerosol and/or INP composition are unknown and proposed a probability density function PDF based approach to predicting INPs at a given freezing temperature.~~

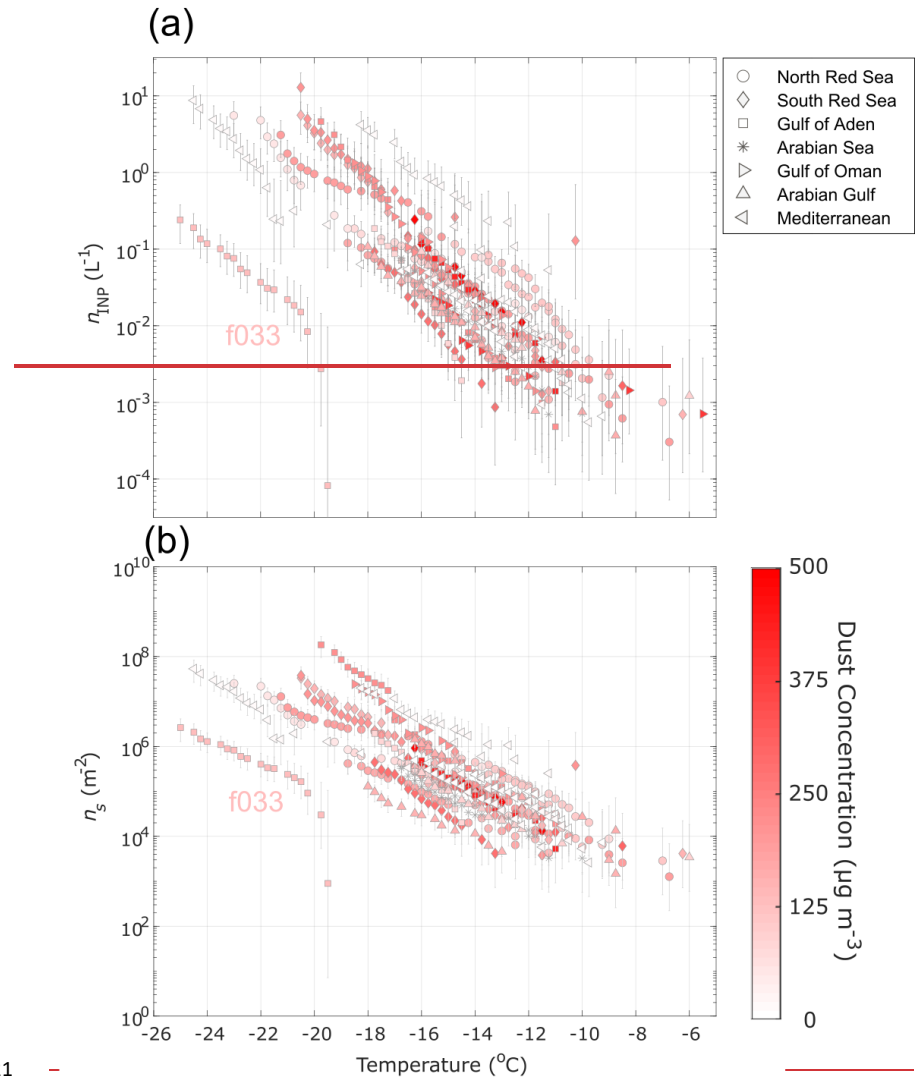
(a)
North Red Sea
South Red Sea
Gulf of Aden
Arabian Sea
Gulf of Oman
Arabian Gulf
Mediterranean
$n_{INP}$ ($L^{-1}$)
f033
(b)
$n_s$ ($m^{-2}$)
f033
Temperature ($^oC$)
Dust Concentration (μg $m^{-3}$)
500
375
250
125
0

621

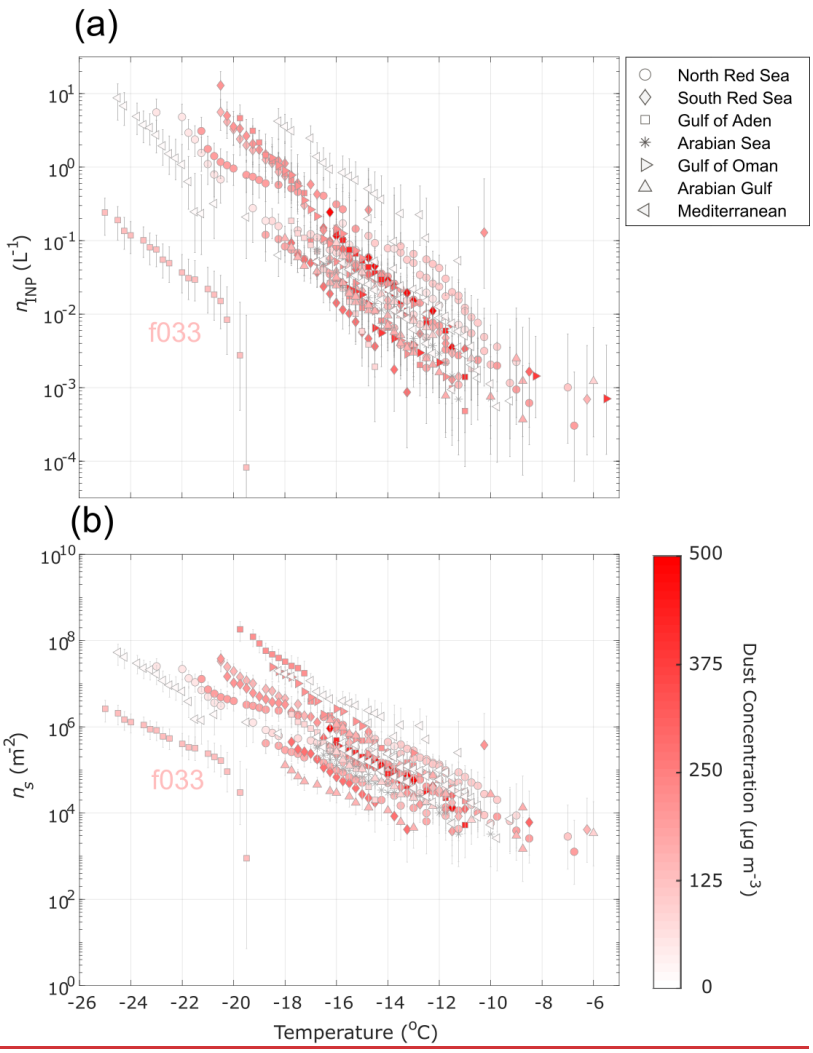


**Figure 43.** INP concentrations ($n_{INP}$) **(a)** and ice ~~nucleation~~-active surface site densities ($n_s$) **(b)** as a function of temperature for 26 aerosol samples collected during AQABA. Markers are colored by the average ambient dust concentration for the respective sampling period. Error bars represent 95% binomial sampling confidence intervals (Agresti and Coull, 1998). The $n_s$ measured in samples collected during low dust conditions are equal to or greater than (up to 100×) the $n_s$

Formatted: Font: Not Italic
Formatted: Font: Not Bold
Formatted: Font: Not Bold
Formatted: Font: Not Bold
Field Code Changed

measured during dust events between -9 and -18 °C. INP concentrations measured in sample f033 were below the detection limits imposed by field blanks (see Sect. 2.4, Fig. S7~~6~~). Sample f020 is not shown in (b) due to missing aerosol surface area data during the sampling period. For the 8 samples on which a dilution was performed (Fig. S8), $n_S$ for both the raw undiluted and diluted sample are shown.

Formatted: Font: Not Bold

Formatted: Font: Not Bold

### 3.4 Characterization of INPs in Aerosol

Formatted: Font: Bold

Offline treatments for testing heat lability and organic composition of INPs were performed on 12 samples via heat and ~~$H_2O_2$~~ peroxide treatments, respectively (Fig. 5~~4~~). Prior studies have shown that the IN-active component of various types of mineral dusts are insensitive to heat treatments (Conen et al., 2011; Hara et al., 2016; Hill et al., 2016; O'Sullivan et al., 2014). The IN activity of K-feldspar, the dominant ice-nucleating~~IN~~ component of mineral dust, was additionally found to be insensitive to digestion with peroxide (O'Sullivan et al., 2014). A small number of studies reported degradation of IN activity with peroxide treatment and/or heat treatment in Arizona Test Dust (ATD), that they attributed to organic material (Perkins et al., 2020; Yadav et al., 2019). Thus, we assume here that any degradation of IN activity due to heat and peroxide treatment ~~are due~~correspond to loss of heat-labile (e.g. proteinaceous) and heat-stable organic INPs, respectively.

Fisher's Exact Test was applied to frozen and unfrozen well fractions for each untreated sample and its corresponding treated sample to test for significant differences ($p < 0.05$). Sensitivity to peroxide in most samples (i.e., INP degradation) demonstrate the consistent presence of stable organic INPs at temperatures ≥ -15 °C. The lack of peroxide sensitivity at temperatures <~~below~~ -15 °C indicates dominance by mineral dust INPs at lower temperatures. Heat sensitivity in five samples suggests that biological INPs contributed to their warmest freezing INPs. Gong et al. (2020) similarly found heat-sensitivity in INPs at temperatures > -10 °C. Four of the 12 samples exhibited heat sensitivity at relatively moderate temperatures -11 to -18 °C, including the two samples collected in the Mediterranean Sea. One sample (f010) exhibited increased $n_{INP}$ ~~INP concentrations~~ in freezing temperatures <~~below~~ -18 °C after heat and peroxide treatments. That the response to both heat and peroxide were nearly identical (Fig. 5~~4~~) suggests that compounds may have been released from the surface during heating, uncovering a more IN active surface

underneath (heating was common to both procedures). The increased $n_{INP}$ post heat and peroxide treatment is an unexpected result given previous studies on treated soil dust measurements (Conen et al., 2011; Hill et al., 2016; O'Sullivan et al., 2014; Tobo et al., 2014). However, increases in IN activity after heat treatment have been reported previously for airborne Saharan desert dust and aerosol collected during Saharan dust intrusions (Boose et al., 2019; Conen et al., 2022) as well as SSA and precipitation (Martin et al., 2019; McCluskey et al., 2018a) and should be further investigated in future studies.~~, though an~~An increase in IN activity after peroxide treatment has

Formatted: Font: Not Italic

also been reported in a Himalayan dust sample (Paramonov et al., 2018). ~~peroxide treatment has also been reported in a Himalayan dust sample (Paramonov et al., 2018).~~

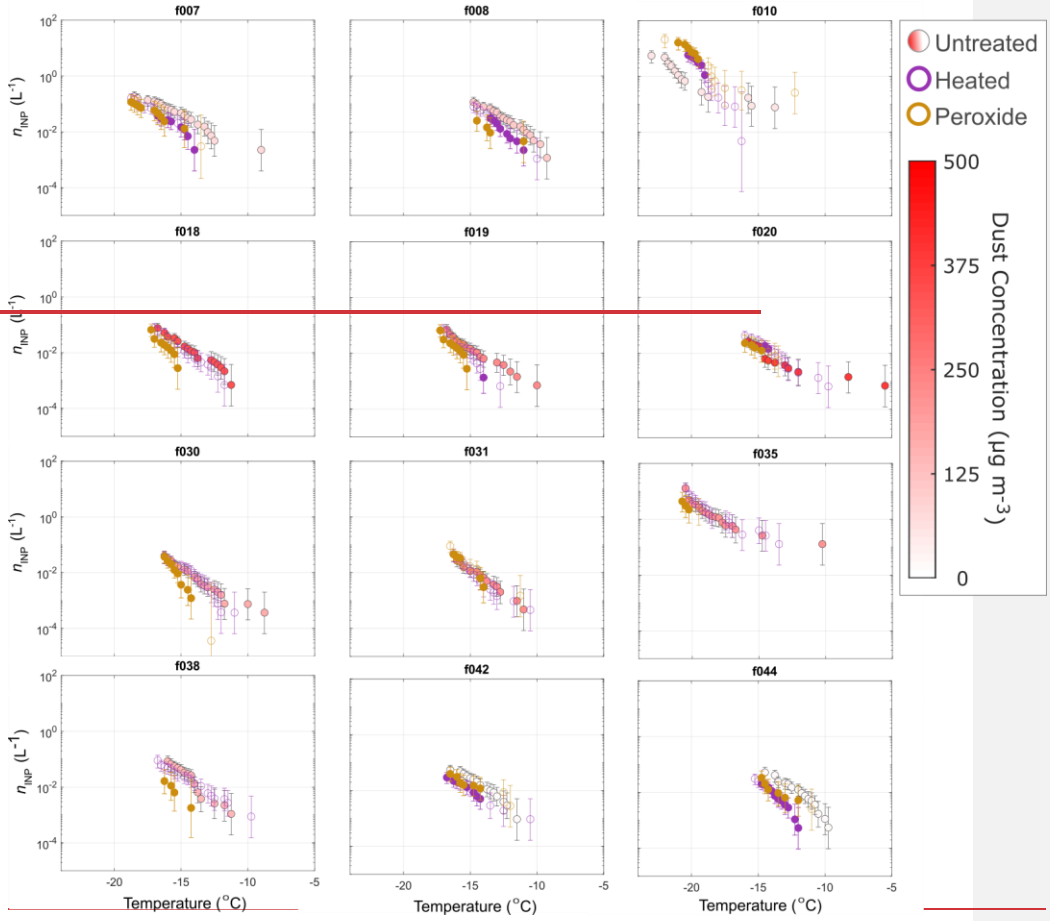
f007
f008
f010
f018
f019
f020
f030
f031
f035
f038
f042
f044
$n_{INP}$ ($L^{-1}$)
Temperature (°C)
Untreated
Heated
Peroxide
Dust Concentration (µg $m^{-3}$)
500
375
250
125
0

666

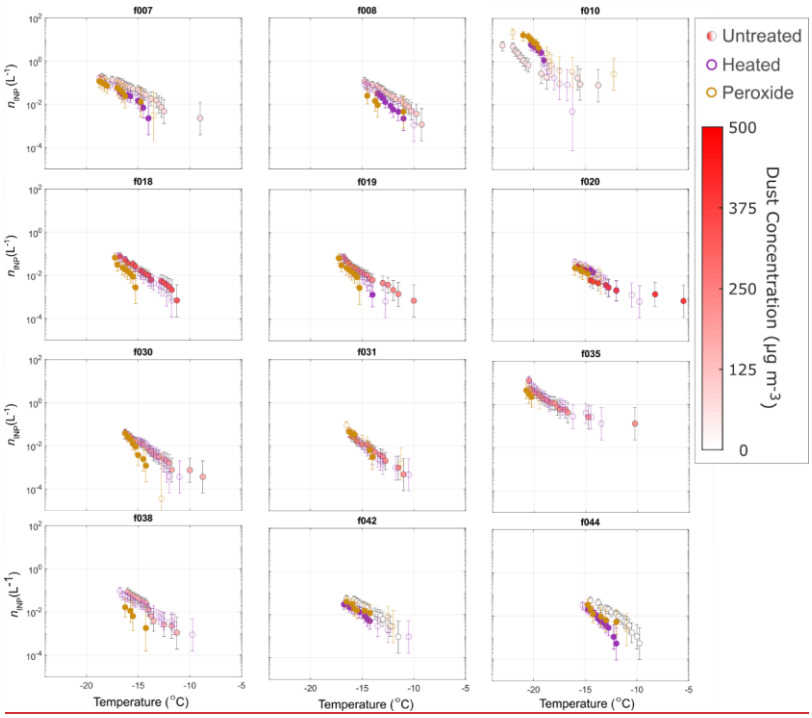


**Figure** ~~5~~**4**. INPs in aerosol samples treated with heat and ~~$H_2O_2$~~ peroxide (Methods Sec. 2.4) to test for INP heat-lability and organic composition. Markers of untreated spectra are colored by the average dust concentration during the sampling period. Markers of heat-treated and ~~$H_2O_2$~~peroxide-treated samples are filled to indicate significant INP concentration difference from untreated samples according to Fisher's Exact Test ($p < 0.05$). Sensitivity to ~~$H_2O_2$~~ peroxide is evident for all samples $\geq$ -15 °C, indicative of stable organic INPs. Heat-lability is also evident at high to moderate temperatures in multiple samples, demonstrating that biological (e.g., proteinaceous) INPs also contributed to INPs observed during AQABA.

Given the frequency of dust ~~storms~~ events and generally high concentrations of dust during most sampling periods, it is surprising that most samples exhibit peroxide sensitivity. Aridisols and entisols are the dominant soil types in North Africa and the Arabian Peninsula (Nortcliff, 2012). Both types are associated with the lowest levels of organic carbon, commonly used as a proxy for

total soil organic matter, compared to other soil types (3 and 9 g $kg^{-1}$, respectively) (Yost and Hartemink, 2019).

### 3.5 Characterization of INPs in a Soil Dust Sample

INP measurements of soil dusts in this region are scarce and have only been reported for a single surface dust soil sample, sample "SD", collected 50 km north of Cairo (Niemand et al., 2012). FLEXPART back-trajectories indicate this source region for several samples (f006-10, f038), though it should be noted that dust sources cannot be confirmed in this study lacking aerosol and soil dust minerology. For comparison with this study, we measured INPs in untreated, heat-treated, and peroxide-treated subsamples of an archived ~~aliquot~~ suspension of the N12-~~-~~SD sample (Methods Sect. 2.4; DeMott et al., 2018) ~~described in~~ . ~~Niemand et al. (2012)~~. Sample N12-SD exhibits sensitivity to both heat and peroxide at temperatures > -16 °C, indicating biological composition of INPs at high freezing temperatures. Multiple AQABA samples influenced by desert air mass sources show similar sensitivities at higher temperatures: f006, f007, f019, and f020. Several others exhibit only peroxide-sensitivity in this temperature range. Overall, the heat and peroxide sensitivities in the N12-SD sample indicate that desert dusts may contribute biological and/or organic INPs at moderate to high-freezing temperatures, such as those observed in AQABA samples. Gong et al.'s (2020) results showing heat-sensitivity in INPs at temperatures > -10 °C further demonstrate the contribution of biological INPs at high temperatures in dust-laden~~y~~ air masses near North~~.~~ Africa.

**Formatted:** Font: Bold
**Formatted:** Font: Bold
**Formatted:** Font: Bold
**Formatted:** Font: (Default) Times New Roman, 12 pt
**Formatted:** Normal
**Formatted:** Font: (Default) Times New Roman, 12 pt, Bold
**Formatted:** Font: (Default) Times New Roman, 12 pt
**Formatted:** Font: (Default) Times New Roman, 12 pt
**Formatted:** Font: (Default) Times New Roman, 12 pt
**Formatted:** Font: (Default) Times New Roman, 12 pt
**Formatted:** Font: (Default) Times New Roman, 12 pt
**Field Code Changed**
**Formatted:** Font: (Default) Times New Roman, 12 pt
**Formatted:** Font: (Default) Times New Roman, 12 pt, Bold
**Formatted:** Font: (Default) Times New Roman, 12 pt
**Formatted:** Font: 14 pt, Bold

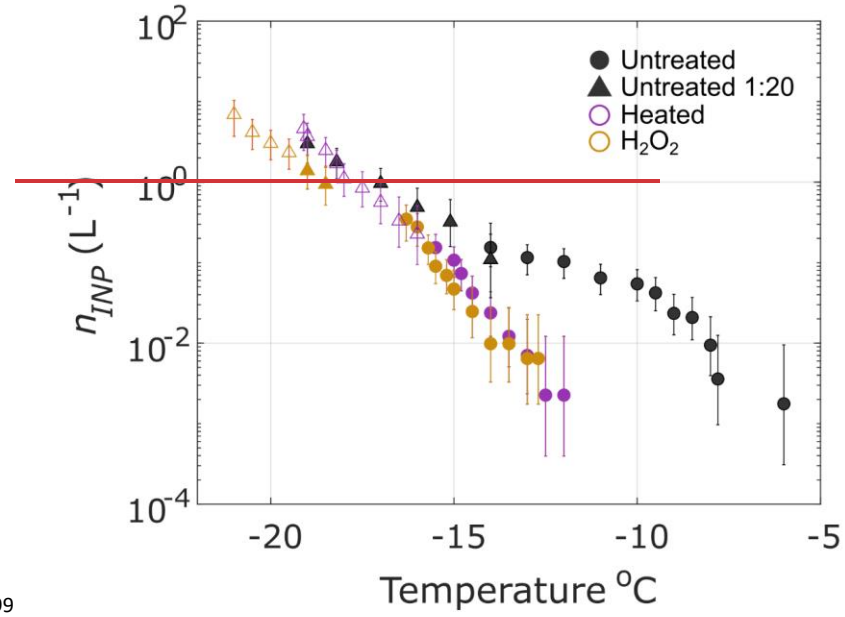
Untreated
Untreated 1:20
Heated
H2O2
$n_{INP}$ (L$^{-1}$)
Temperature °C

699

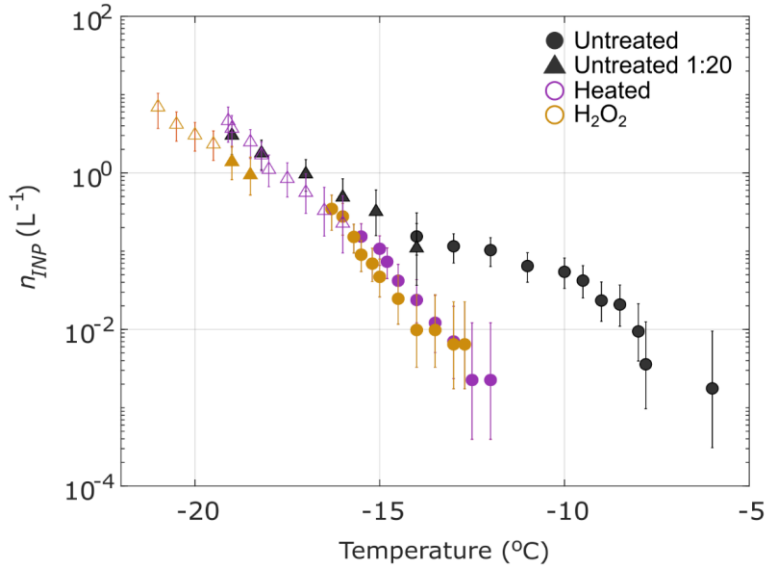
Untreated
Untreated 1:20
Heated
H2O2
$n_{INP}$ (L$^{-1}$)
Temperature (°C)

700

**Figure 6~~5~~.** Measured concentrations of INPs in an aerosolized soil dust sample "N12-SD", collected 50 km north of Cairo, Egypt (Niemand et al., 2012), that was treated with heat and peroxide to test for INP heat-lability and organic composition, same as in Fig. 5~~4~~ above (Methods Sec. 2.4). A 1:20 dilution of the sample is shown (triangles) and markers of heat-treated and ~~$H_2O_2$~~peroxide-treated samples are filled to indicate significant INP concentration differences from untreated samples according to Fisher's Exact Test ($p < 0.05$). Sensitivity to peroxide and heat treatments indicates biological INPs between -6 and -16 °C.

## 4 Discussion

Considering the high freezing temperatures observed, evidence of organic composition, and FLEXPART back trajectories showing that aerosol sources included populous regions and at least one agriculturally active region (the Nile River Delta; Figs. S9-S16), it is possible that agricultural soil dusts contributed to some of the relatively higher $n_s$, $n_{INP}$, and heat and peroxide sensitivity observed during AQABA. A range of $n_s$ has been reported in studies of agricultural soil dusts, the lower end of which agrees with the $n_s$ observed in the present study between -8 and -25 °C (Fig. 3; Steinke et al., 2016; Tobo et al., 2014; O'Sullivan et al., 2014). Samples from air masses influenced by the Nile River Delta or Southern Europe (f007-8, f010, f038, f042, f044) show a higher fraction of heat-sensitive INPs (Fig. 5~~4~~). Heat-sensitivity is indicative of biological INPs, which have been associated with agricultural soil dusts in prior studies (Hill et al., 2016; O'Sullivan et al., 2014). Hill et al. (2016) and O'Sullivan et al. (2014) showed peroxide sensitivity in agricultural soil dusts at temperatures > -18 to -15 °C, respectively, a range which aligns with the peroxide sensitivity exhibited in the present study. ~~A range of $n_s$ has been reported in studies of agricultural soil dusts, the lower end of which agrees with the $n_s$ observed in the present study between -8 and -25 °C (Steinke et al., 2016; Tobo et al., 2014; O'Sullivan et al., 2014). Agricultural soil dusts are relatively rich in organic and biological material (Conen et al., 2011, 2016; Ellerbrock et al., 2005; Kögel-Knabner et al., 2008; O'Sullivan et al., 2014) and contribute up to 20-25% of the global dust load (Ginoux et al., 2012). Furthermore, they are associated with IN activities higher than that of mineral dust (Conen et al., 2011; Fornea et al., 2009; Isono and Ikebe, 1960; O'Sullivan et al., 2014; Steinke et al., 2016; Tobo et al., 2014). High onset temperatures, up to -6 °C, are the norm (Conen et al., 2011; Garcia et al., 2012; Hill et al., 2016; O'Sullivan et al., 2014),~~

Formatted: Font: Bold

Formatted: Font: Not Italic

~~and the high activity of agricultural soil particles has been attributed to internally mixed organic matter (O'Sullivan et al., 2014; Tobo et al., 2014).~~

Organic material can condense or adsorb onto aerosols during photochemical and oxidative processes, representing another potential source of organic INPs during AQABA (Dall'Osto et al., 2010; Hinz et al., 2005; Krueger et al., 2004). Could aging explain the organics and decreased $n_s$ observed? Though dust aerosol was collected within 1 day's transport from source regions throughout this study, we cannot rule out the possibility of aging impacts, lacking single particle chemistry measurements ~~(e.g., Sullivan et al., 2007)~~. In addition to field observations of $n_{INP}$ ~~INP concentrations~~ demonstrating that aging increased the IN efficiency of desert dust INPs (see Introduction; Boose et al., 2016; Conen et al. 2015), prior studies of the effects of aging on mineral dust INPs have yielded mixed and sometimes contradictory results, indicating that the impact of aging on IN properties likely depends on multiple factors including the ice nucleation pathway, the type of aging process, surface morphology, and mineralogy (Perkins et al., 2020 and references therein). Multiple studies have investigated the effects of various aging processes on Arizona Test Dust (ATD) as a proxy for diverse natural dust samples. These included exposure to sulfuric acid, nitric acid vapor, and solution-phase processes (Cziczo et al., 2009; Eastwood et al., 2009; Knopf and Koop, 2006; Salam et al., 2007; Sullivan et al., 2010b, 2010a). Perkins et al. (2020) demonstrated the INP lability in ATD through multiple solution-phase aging processes (e.g., incubation in water, exposure to acid or salt), with up to 1000× ~~fold~~ reductions in INP abundance at freezing temperatures > 10 °C. This result contrasts with the increase in IN activity attributed to aging reported in Boose et al. (2016) and Conen et al. (2015). Perkins et al. (2020) additionally reported that the lability of IN activity in ATD is temperature dependent, with large reductions evident at freezing temperature > 10 °C, yet little to no change at temperatures <~~below~~ -15 °C. By contrast, most of the $n_s$ spectra in AQABA samples were 10 – 1000× lower than established dust parameterizations even at temperatures < ~~below~~ -15 °C. In summary, it has proven difficult to determine any consistent impact of atmospheric processing on the IN activity of dust in model systems such as ATD (Perkins et al., 2020), and few studies have investigated impacts of aging on ambient desert dust, especially at modest supercooling (Boose et al., 2016). Furthermore, the use of ATD as a proxy for natural dust in INP studies has been questioned due to the complex ice-nucleating ~~IN~~ properties of natural dust, including mineral composition and defect sites at the

Field Code Changed

particle surface, the latter of which is likely affected by the mechanical processing and milling involved in ATD production (e.g., Perkins et al., 2020 and references therein).

~~Gong et al. (2020) also observed $n_s$ lower by more than 2 orders of magnitude compared to N12 and U17 despite the large fraction of supermicron INPs (77-83% depending on temperature), and that the supermicron particles were mainly mineral dust. The large differences between parameterized $n_s$ for dust, and $n_s$ observed in both Gong et al. (2020) and the present study between -12 and -25 °C demonstrate that existing $n_s$-based parameterizations may not faithfully represent $n_s$ at moderate freezing temperatures, despite proximity to major source regions. Whereas DeMott et al. (2015a) found that for temperatures < -20 °C, mineral dust particles from Saharan and Asian deserts may be parameterized as a common particle type, our findings suggest that characteristic $n_s$ parameterizations for dust from different source regions may be needed > -20 °C, or, alternatively, that this temperature regime requires an alternative to an $n_s$-based parameterizations. Gong et al. (2019a) demonstrated that predicting $n_{INP}$ from surface area size distributions alone may not be feasible in environments where the aerosol and/or INP composition are unknown and proposed a probability density function PDF-based approach to predicting INPs at a given freezing temperature.~~

Gong et al. (2020) also observed $n_s$ lower by more than 2 orders of magnitude compared to N12 and U17 despite the large fraction of supermicron INPs (77-83% depending on temperature), and that the supermicron particles were mainly mineral dust. The cause of the decreased $n_s$ observed here and in Gong et al. (2020) compared to dust $n_s$ parameterizations remains elusive. Both studies were conducted in air masses dominated by dust near major sources. In contrast, Price et al. (2018) found agreement near the region of the Gong et al. (2020) study. One obvious difference is that Price et al. (2018) conducted measurements at higher altitudes, between 30 and 3500 m. A prior study that compared $n_{INP}$ in dust-laden air masses at the surface with $n_{INP}$ collected between 0.5 and 3 km above sea level found that median $n_{INP}$ increased by up to 10× above the surface and correlated to dust loading (Schrod et al., 2017). The differences between Price et al. (2018) and

**Formatted:** Font: Not Italic

**Formatted:** Font: Not Italic

**Formatted:** Font: Not Italic

the two surface-based studies draws attention to the need for vertical profiles of $n_s$ > -25 °C in dust-laden air masses.

The decreased $n_s$ compared to Price et al. (2018) is also unlikely to be related to differences in INP measurement. In all three studies, cold stage or droplet assay measurements of immersion mode INPs were used in resuspensions of aerosol collected on filter samples. Recent studies that intercompared instruments designed for measurement of immersion mode INPs showed excellent agreement (i.e., within measurement uncertainty) in measurements of standardized dust and biological samples (DeMott et al., 2018) and when co-sampling ambient aerosol (DeMott et al., 2017). Moreover, the DeMott et al. (2018) intercomparison study demonstrated good agreement in multiple natural dust samples between the various measurement methods used to derive D15, N12 and U17 and the droplet assay methods applied in Gong et al. (2020), Price et al. (2018)~~),~~ and the present study.

Storage protocol represents another difference between ~~(~~Price et al.~~,~~ (2018) and the two surface-based studies. ~~(~~Gong et al.~~,~~ (2020) and the present study stored samples frozen prior to analysis, whereas ~~(~~Price et al.~~,~~ (2018) processed samples immediately after collection. An understanding of storage impacts on INPs collected on filters is lacking (Wex et al., 2019), but we note that the discrepancies in $n_s$ between the two surface-based studies and ~~(~~Price et al.~~,~~ (2018) exceed the range of INP concentration changes reported in untreated INP precipitation samples stored frozen (Beall et al., 2020).

Thus, the large differences between parameterized $n_s$ for dust, and $n_s$ observed in both Gong et al. (2020) and the present study between -12 and -25 °C indicate that existing $n_s$-based parameterizations may not faithfully represent $n_s$ at moderate freezing temperatures, despite proximity to major source regions. Whereas DeMott et al. (2015) found that for temperatures < -20 °C, mineral dust particles from Saharan and Asian deserts may be parameterized as a common particle type, our findings suggest that characteristic $n_s$ parameterizations for dust from different source regions may be needed > -20 °C, or, alternatively, that this temperature regime requires an alternative to an $n_s$-based parameterizations. Gong et al. (2019a) demonstrated that predicting $n_{INP}$ from surface area size distributions alone may not be feasible in environments where the aerosol and/or INP composition are unknown and proposed a probability density function (PDF)-based

**Formatted:** No widow/orphan control, Don't keep with next

**Formatted:** Font: Not Italic

approach to predicting INPs at a given freezing temperature.

In light of the evidence from this study that INPs were primarily influenced by organics associated with dust, especially at higher temperatures, and the lack of relationship between dust loading, $n_s$, and $n_{INP}$, we offer the following points for consideration. ~~—~~Prior studies of aerosolized dust demonstrated that it is frequently enriched in organic matter (6-20×) compared to soil dust~~×~~ and that wind erosion selectively removes the chemically-enriched, fine portion of the soil higher ~~of~~ in plant nutrients, organic matter and metals (Aryal et al., 2012; Delany and Zenchelsky, 1976; Van Pelt and Zobeck, 2007). Furthermore, a recent study that measured airborne concentrations of prokaryotic cells over the Red Sea characterized the region as a "global hot spot" with average concentrations of 155,000 (± 65,000) cells $m^{-3}$, 19× higher than that over the subtropical and tropical open oceans (Mayol et al., 2014; Yahya et al., 2019). Yahya et al. (2019) demonstrated that the microbial loading was very likely related to the high concentrations of dust, as 99.9% of the cells were attached to dust particles. Organic and biological species have been shown to dominate IN activity at temperatures > ~-15 °C in many studies (e.g., ~~Kanji et al., 2017;~~ Ladino et al., 2019; O'Sullivan et al., 2018, Kanji et al., 2017, and references therein). Thus, a faithful representation of dust INPs may require two parameterizations: one for the IN activity dominated by minerals < ~-15 °C such as D15, U17 and N12, and another for the dust-associated organics > ~-15 °C. As IN-active organics are limited compared to the IN-active mineral component of dust, we could expect an increase in $n_s$ slope between warm and cold regimes. The apparent decreased $n_s$ observed in this study between -18 and -12 °C could potentially be related to a plateau in $n_s$ through the transition between the mineral and organic "modes" (see untreated samples in Figs. 5-~~Fig.~~ 6~~5~~). This study underscores the need to characterize the IN-active organic species associated with dust from major source regions and to investigate the extent to which biological and/or organic particles contribute to INP populations in dust-laden air masses at high to moderate freezing temperatures ≥ -15 °C.

### ~~3.2 Seawater Source Potential~~

~~The $n_{INP}$ values in 10 SSW samples collected during AQABA were used to characterize the INP source potential of SSA generated by bubble bursting (Wang et al., 2017). Results from prior studies have demonstrated that jet droplets are a more efficient transfer vehicle than film drops of~~

Formatted: Font: Not Italic

Formatted: Superscript

Formatted: Justified

INPs into SSA particles (Mitts et al., 2021; Wang et al., 2017). While it is unlikely that many of the INPs detected in aerosol samples were marine in origin (see Sec. 3.1), we measured the INP concentrations in SSW to test whether the seawater source strength was comparable to that of prior studies, or were possibly enriched with INPs due to biological activity or even dust deposition (Cornwell et al., 2020).

Figure S10 shows how the INP concentrations measured at -19 °C in 10 seawater samples varied by the sample collection location. Concentrations ranged between 1 and 50 INPs $mL^{-1}$ and were highest between the Gulf of Oman and the Gulf of Aden. This region exhibited relatively high chlorophyll *a* during the cruise, with levels between 1 and 30 mg $m^{-3}$ (Fig. S11). In Fig. 6, INP concentrations were compared with SSW from the Ellen Browning Scripps Memorial Pier in coastal Southern California (SIO Pier), Cabo Verde in the Northeast Atlantic, the Southern Ocean (McCluskey et al., 2017), and the Northwest Atlantic (Schnell, 1977). AQABA INP concentrations were most comparable with Gong et al.'s (2020) observations in Cabo Verde. The

lack of any unusually high INP spectra suggests that INP enrichment due to dust deposition (Cornwell et al. 2020) was absent or infrequent.

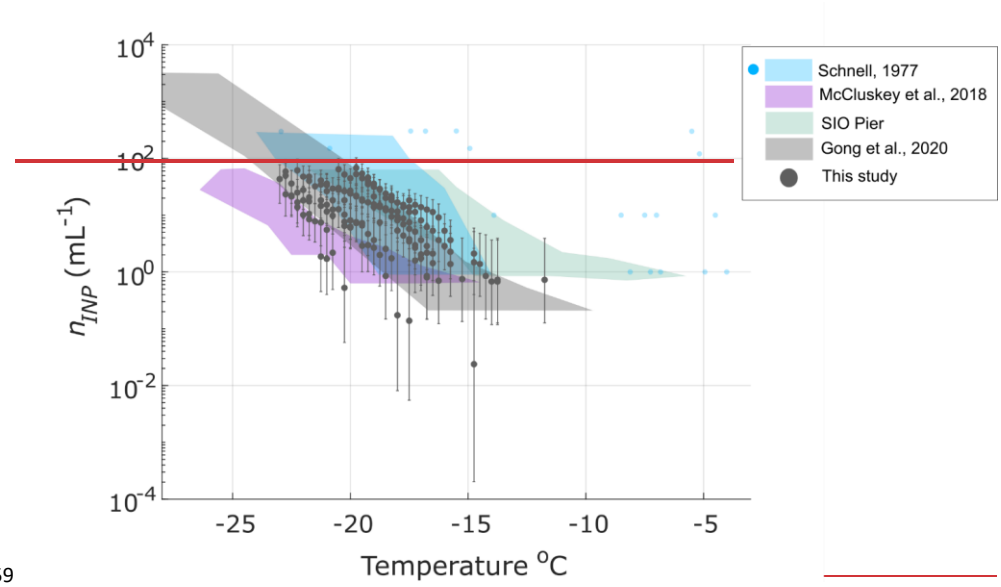


**Figure 6.** Measured INP concentrations in 10 SSW samples collected during AQABA. Also shown are the composite INP spectrum of coastal SSW samples collected on São Vincente Island, Cabo Verde (Gong et al., 2020), coastal SSW samples collected at the Ellen Browning Scripps Pier (green shading), and SSW samples collected in the Southern Ocean (McCluskey et al., 2018d). Schnell's (1977) SSW measurements are represented as a composite spectrum of 24 samples (blue shaded region) and 5 additional spectra (blue markers) from samples that exhibited higher freezing temperatures. All spectra presented are uncorrected for freezing point depression. Offline treatments for testing heat lability, organic composition, and size were applied to 5 of the 10 seawater samples (Methods Sec. 2.4). Heat and 0.2 µm filtering treatments suggest that a large fraction of the seawater INPs were heat sensitive and larger than 0.2 µm. These results are indicative of the particulate organic carbon (POC) type of marine INP defined in McCluskey et al. (2018a) (Fig. S12).

Formatted: Font: (Default) Times New Roman, 12 pt

~~Heat-resilience but peroxide-sensitivity in sample s001 additionally indicates the presence of non-proteinaceous organic INPs, such as the dissolved organic carbon (DOC) type defined in McCluskey et al. (2018a). Considering the characteristically low IN activity of the SSW, the lower $n_s$ of SSA compared to mineral dust (McCluskey et al., 2018b), and the frequency of dust events during AQABA, our findings suggest that dust was highly likely to be the dominant INP class observed in this study.~~

## ~~5~~4 Conclusions

Observations from the two-month AQABA campaign in the Mediterranean, Red Sea, Arabian Sea and Arabian Gulf are among the first INP measurements made in close proximity to the two largest dust sources globally: the Sahara and the Arabian Peninsula (Kok et al., 2021). Observed $n_{INP}$ ~~INP concentrations~~ measured in 26 aerosol samples spanned ~~two~~ 2 ~~or more~~ orders of magnitude (5 × $10^{-3}$ to 5 × $10^{-1}$ $L^{-1}$ ~~0.002 to 0.5 $L^{-1}$~~ at -15 °C).

In summary, INPs observed during AQABA were very likely dominated by mineral dust with some additional contributions possibly from densely-populated and/or agricultural regions including the Nile River Delta region and Southern or Eastern Europe. Despite proximity to major dust sources and a high frequency of dust events with MERRA-2 simulated mass concentrations up to 490 µg $m^{-3}$ ($PM_{10}$), the observed $n_s$ for most samples was lower by 1-3 orders of magnitude compared to $n_s$ predicted by dust parametrizations N12 and U17 at T < -12 °C ~~(Niemand et al., 2012; Ullrich et al., 2017)~~. Observed $n_s$ in 48% of the samples were equivalent within uncertainty to that of ~~Many INPs measured in AQABA showed agreement with~~ the A13 parameterization for K-feldspar (Atkinson et al., 2013), an ice-active component of desert dust. Observed $n_s$ agreed ~~,~~ ~~with~~ with many observations within the marine boundary layer (DeMott et al., 2016; Yang et al., 2020), and ~~with the~~ Price et al.'s (2018) measurements of $n_{INP}$ ~~INP concentrations~~ in dust-laden air masses over the Tropical Atlantic, within measurement uncertainty. Peroxide sensitivity was evident in all samples tested (12 of 26), at temperatures ≥ -15 °C, demonstrating a consistent contribution of organic material to warm-temperature INPs. Heat-sensitivity further suggested the presence of biological (e.g., proteinaceous) INPs in a subset of samples, particularly at high freezing temperatures > -10 °C. ~~While the dominant mineral dusts in the region are associated with~~

**Formatted:** Font: Italic
**Formatted:** Subscript
**Formatted:** Font: Not Bold
**Formatted:** Font: Not Bold
**Formatted:** Font: Not Bold
**Formatted:** Font: Not Bold

~~the lowest concentrations of soil organic carbon globally (e.g., Yost and Hartemink, 2019 and references therein), aerosolized fine dust is known to be enriched in organic matter (Aryal et al., 2012; Delany and Zenchelsky, 1976; Van Pelt and Zobeck, 2007) and is additionally associated with high microbial loading in the Red Sea (Yahya et al., 2019).~~ A soil dust sample from North Africa (originally from N12) exhibited heat and peroxide sensitivity between -5 and -16 °C, further demonstrating that the IN activity of mineral dust could be associated with organic and/or biological material. Contrary to Price et al. (2018), who measured INP in the dust-laden Tropical Atlantic, no correlation was found between dust loading and $n_{INP}$ or $n_s$. Results from this study and Gong et al. (2020) indicate that the existing $n_s$ parameterizations alone do not skillfully represent mineral dust associated INPs at modest supercooling near major dust sources.

The source strengths of Red Sea, Mediterranean, Arabian Sea, and Arabian Gulf bulk seawater were also evaluated. The maximum source potential was observed in the Arabian Sea (50 INP $mL^{-1}$ at -19 °C).) ~~Overall, the~~The observed $n_{INP}$ ~~range~~ for SSW samples were equivalent to ~~agreed well with the~~those of Gong et al. (2020) ~~SSW measurements~~ at Cabo Verde within the 95% binomial sampling confidence intervals (Agresti and Coull, 1998).

Considering that desert dust parameterizations overpredicted the $n_s$ values observed during AQABA, despite proximity to major global emissions sources, this study demonstrates the need to evaluate the fidelity of dust INP parameterizations in nascent versus aged dust populations. The discrepancies underscore the challenges of evaluating dust-specific INP parameterizations: limited observations at modest supercooling, few assured methods for distinguishing between different INP sources in ambient aerosol, a dearth of characteristic soil dust samples from major dust sources, and limited knowledge of the specific composition and characteristics of dust INPs at temperatures > -15 °C. Vertical profiles of $n_s$ in dust-laden air masses are also needed to determine whether $n_s$ is consistently lower at the surface and examine the variability of $n_s$ with altitude. Potential storage impacts on INPs collected on filters are an additional factor worthy of future investigation, though storage alone does not likely explain the relatively decreased $n_s$ compared to parameterizations observed in this study, as U17 and N12 were both derived from stored dust samples.

Formatted: Font: Not Italic

Formatted: Font: Not Italic

Formatted: Font: Not Bold

Formatted: Line spacing: 1.5 lines

Formatted: Font: (Default) Times New Roman, 12 pt

Formatted: Font: (Default) Times New Roman, 12 pt

Formatted: Font: (Default) Times New Roman, 12 pt

Formatted: Font: (Default) Times New Roman, 12 pt

In addition to providing observations at high to moderate freezing temperatures, future studies could apply the methods developed in Gong et al. (2020) to estimate the contribution of marine INPs to the aerosol sampled by assuming equivalent distributions of sea salt and INPs between seawater and air. Furthermore, given the combination of marine, dust, and anthropogenically-influenced air masses encountered, and the evidence of organic and biological INPs at modest supercooling in this study and Gong et al. (2020), future studies could benefit from advances in on-line Light-Induced Fluorescence (LIF) measurement techniques. Whereas the interpretation of fluorescence data from most LIF-based instruments has been limited by the lack of spectroscopic information, newer instruments support real-time spectrally-resolved size and fluorescence measurement information for single particles (Fennelly et al., 2018; Huffman et al., 2020; Könemann et al., 2019). This information could be used to potentially "tag" different classes of organics and biological aerosols, enabling investigations of relationships between $n_s$, $n_{INP}$ and organic signatures in, e.g., mineral dusts and agricultural soil dusts. Finally, the decreased $n_s$ observed in this study further motivate comprehensive aerosol-ice nucleation studies, which aim to achieve closure between measured and predicted ambient $n_{INP}$ ~~INP concentrations~~ by simultaneously characterizing ambient INPs and ice nucleation relevant properties of the total aerosol population, such as composition and aerosol chemical mixing state (Sullivan et al., 2007).

**Data Availability**: The data set supporting this manuscript is hosted by the UCSD Library Digital Collections (**https://doi.org/10.6075/J0X0676P**) (Beall et al., 2021).

**Author contributions:**

CMB, TCH, PJD, MOA, CP, JL, JS, FD, BW, HH, MDS, and KAP designed the study. CMB performed the INP measurements, FLEXPART modeling and analysis with support from TCH, PJD, MOA, MDS, MP and KAP. TCH, PJD and MOA contributed significantly to the writing, preparation of figures and analysis. TK, MI, RP and HH supported the field collection of aerosol for INP analysis and TK additionally provided aerosol number concentration data. JS and MP

Formatted: Font: Not Italic

Formatted: Font: 12 pt

Formatted: Font: 12 pt

Formatted: Font: 12 pt

provided aerosol water-soluble composition data. FD oversaw the aerosol sizing and AMS composition measurements and analysis. All authors contributed to the writing of the article.

**Competing interests:**

The authors declare they have no conflict of interest.

**Acknowledgements:**

The authors acknowledge collaborations with King Abdullah University of Science and Technology (KAUST), the Cyprus Institute (CyI) and the Kuwait Institute for Scientific Research (KISR). We additionally thank Marcel Dorf and Claus Koeppel for the organization of the campaign, as well as Horst Fischer, Ivan Tadic and Uwe Parchatka for provision of the NO data. Analyses and visualizations of dust mass concentrations and Chl *a* used in this paper were produced with the Giovanni online data system, developed and maintained by the NASA GES DISC. Maps throughout this article were created using ArcGIS® software by Esri. We would also like to thank Hays Ships Ltd. and the *Kommandor Iona*'s crew for their attention to the safety and well-being of the researchers. Finally, we thank the three anonymous reviewers whose insightful comments strengthened this paper. Funding was provided by Highly Cited Program at King Saud University and the Max Planck Society and the University of California San Diego (UCSD) Understanding and Protecting the Planet initiative.

Formatted: Font: 12 pt

Formatted: Font: (Default) Times New Roman, 12 pt

**References**

Agresti, A. and Coull, B. A.: Approximate Is Better than "Exact" for Interval Estimation of Binomial Proportions, Am. Stat., 52(2), 119, doi:10.2307/2685469, 1998.

Ardon-Dryer, K. and Levin, Z.: Ground-based measurements of immersion freezing in the eastern Mediterranean, Atmos. Chem. Phys., 14(10), 5217–5231, doi:10.5194/acp-14-5217-2014, 2014.

Aryal, R., Kandel, D., Acharya, D., Chong, M. N. and Beecham, S.: Unusual Sydney dust storm and its mineralogical and organic characteristics, Environ. Chem., 9(6), 537–546 [online] Available from:

https://doi.org/10.1071/EN12131, 2012.

Atkinson, J. D., Murray, B. J., Woodhouse, M. T., Whale, T. F., Baustian, K. J., Carslaw, K. S., Dobbie, S., O'Sullivan, D. and Malkin, T. L.: The importance of feldspar for ice nucleation by mineral dust in mixed-phase clouds, Nature, 498(7454), 355–358, doi:10.1038/nature12278, 2013.

Beall, C. M., Stokes, M. D., Hill, T. C., DeMott, P. J., DeWald, J. T. and Prather, K. A.: Automation and Heat Transfer Characterization of Immersion Mode Spectroscopy for Analysis of Ice Nucleating Particles, Atmos. Meas. Tech., (February), 1–25, doi:10.5194/amt-2016-412, 2017.

Beall, C. M., Lucero, D., Hill, T. C., DeMott, P. J., Stokes, M. D. and Prather, K. A.: Best practices for precipitation sample storage for offline studies of ice nucleation in marine and coastal environments, Atmos. Meas. Tech., 13(12), 6473–6486, doi:10.5194/amt-13-6473-2020, 2020.

Beall, C. M., Michaud, J. M., Fish, M. A., Dinasquet, J., Cornwell, G. C., Stokes, M. D., Burkart, M. D., Hill, T. C., Demott, P. J. and Prather, K. A.: Cultivable halotolerant ice-nucleating bacteria and fungi in coastal precipitation, Atmos. Chem. Phys., 21(11), 9031–9045, doi:10.5194/acp-21-9031-2021, 2021.

Boose, Y., Sierau, B., Isabel García, M., Rodríguez, S., Alastuey, A., Linke, C., Schnaiter, M., Kupiszewski, P., Kanji, Z. A. and Lohmann, U.: Ice nucleating particles in the Saharan Air Layer, Atmos. Chem. Phys., 16(14), 9067–9087, doi:10.5194/acp-16-9067-2016, 2016.

Boose, Y., Baloh, P., Plötze, M., Ofner, J., Grothe, H., Sierau, B., Lohmann, U. and Kanji, Z. A.: Heterogeneous ice nucleation on dust particles sourced from nine deserts worldwide -- Part 2: Deposition nucleation and condensation freezing, Atmos. Chem. Phys., 19(2), 1059–1076, doi:10.5194/acp-19-1059-2019, 2019.

Bourtsoukidis, E., Ernle, L., Crowley, J. N., Lelieveld, J., Paris, J.-D., Pozzer, A., Walter, D. and Williams, J.: Non-methane hydrocarbon (\chem{C_2}--\chem{C_8}) sources and sinks around the Arabian Peninsula, Atmos. Chem. Phys., 19(10), 7209–7232, doi:10.5194/acp-19-7209-2019, 2019.

Bourtsoukidis, E., Pozzer, A., Sattler, T., Matthaios, V. N., Ernle, L., Edtbauer, A., Fischer, H., Könemann, T., Osipov, S., Paris, J.-D., Pfannerstill, E. Y., Stönner, C., Tadic, I., Walter, D., Wang, N., Lelieveld, J. and Williams, J.: The Red Sea Deep Water is a potent source of atmospheric ethane and propane, Nat. Commun., 11(1), 447, doi:10.1038/s41467-020-14375-0, 2020.

Broadley, S. L., Murray, B. J., Herbert, R. J., Atkinson, J. D., Dobbie, S., Malkin, T. L., Condliffe, E. and Neve, L.: Immersion mode heterogeneous ice nucleation by an illite rich powder representative of atmospheric mineral dust, Atmos. Chem. Phys., 12(1), 287–307, doi:10.5194/acp-12-287-2012, 2012.

1012 Brunner, C., Brem, B. T., Collaud Coen, M., Conen, F., Hervo, M., Henne, S., Steinbacher, M., Gysel-
1013 Beer, M. and Kanji, Z. A.: The contribution of Saharan dust to the ice-nucleating particle concentrations
1014 at the High Altitude Station Jungfraujoch (3580\,m\,a.s.l.), Switzerland, Atmos. Chem. Phys., 21(23),
1015 18029–18053, doi:10.5194/acp-21-18029-2021, 2021.

1016 Buchard, V., Randles, C. A., da Silva, A. M., Darmenov, A., Colarco, P. R., Govindaraju, R., Ferrare, R.,
1017 Hair, J., Beyersdorf, A. J., Ziemba, L. D. and Yu, H.: The MERRA-2 Aerosol Reanalysis, 1980 Onward.
1018 Part II: Evaluation and Case Studies, J. Clim., 30(17), 6851–6872, doi:10.1175/JCLI-D-16-0613.1, 2017.

1019 Burrows, S. M., Hoose, C., Pöschl, U. and Lawrence, M. G.: Ice nuclei in marine air: biogenic particles or
1020 dust?, Atmos. Chem. Phys., 13(1), 245–267, doi:10.5194/acp-13-245-2013, 2013.

1021 Celik, S., Drewnick, F., Fachinger, F., Brooks, J., Darbyshire, E., Coe, H., Paris, J.-D., Eger, P. G.,
1022 Schuladen, J., Tadic, I., Friedrich, N., Dienhart, D., Hottmann, B., Fischer, H., Crowley, J. N., Harder, H.
1023 and Borrmann, S.: Influence of vessel characteristics and atmospheric processes on the gas and particle
1024 phase of ship emission plumes: in situ measurements in the Mediterranean Sea and around the Arabian
1025 Peninsula, Atmos. Chem. Phys., 20(8), 4713–4734, doi:10.5194/acp-20-4713-2020, 2020.

1026 Collins, D. B., Zhao, D. F., Ruppel, M. J., Laskina, O., Grandquist, J. R., Modini, R. L., Stokes, M. D.,
1027 Russell, L. M., Bertram, T. H., Grassian, V. H., Deane, G. B. and Prather, K. A.: Direct aerosol chemical
1028 composition measurements to evaluate the physicochemical differences between controlled sea spray
1029 aerosol generation schemes, Atmos. Meas. Tech., 7(11), 3667–3683, doi:10.5194/amt-7-3667-2014,
1030 2014.

1031 Conen, F., Morris, C. E., Leifeld, J., Yakutin, M. V and Alewell, C.: Biological residues define the ice
1032 nucleation properties of soil dust, Atmos. Chem. Phys., 11(18), 9643–9648, doi:10.5194/acp-11-9643-
1033 2011, 2011.

1034 Conen, F., Rodríguez, S., Hüglin, C., Henne, S., Herrmann, E., Bukowiecki, N. and Alewell, C.:
1035 Atmospheric ice nuclei at the high-altitude observatory Jungfraujoch, Switzerland, Tellus, Ser. B Chem.
1036 Phys. Meteorol., 67(1), 1–10, doi:10.3402/tellusb.v67.25014, 2015.

1037 Conen, F., Einbock, A., Mignani, C. and Hüglin, C.: Measurement report: Ice-nucleating particles active
1038 $\ge -15$\,{\degree}C in free tropospheric air over western Europe, Atmos. Chem. Phys., 22(5), 3433–
1039 3444, doi:10.5194/acp-22-3433-2022, 2022.

1040 Cornwell, G. C., McCluskey, C. S., Levin, E. J. T., Suski, K. J., DeMott, P. J., Kreidenweis, S. M. and
1041 Prather, K. A.: Direct Online Mass Spectrometry Measurements of Ice Nucleating Particles at a California
1042 Coastal Site, J. Geophys. Res. Atmos., 124(22), 12157–12172, doi:doi:10.1029/2019JD030466, 2019.

Cornwell, G. C., Sultana, C. M., Prank, M., Cochran, R. E., Hill, T. C. J., Schill, G. P., DeMott, P. J., Mahowald, N. and Prather, K. A.: Ejection of Dust From the Ocean as a Potential Source of Marine Ice Nucleating Particles, J. Geophys. Res. Atmos., 125(24), e2020JD033073, doi:https://doi.org/10.1029/2020JD033073, 2020.

Cziczo, D. J., Froyd, K. D., Gallavardin, S. J., Moehler, O., Benz, S., Saathoff, H. and Murphy, D. M.: Deactivation of ice nuclei due to atmospherically relevant surface coatings, Environ. Res. Lett., 4(4), 44013, doi:10.1088/1748-9326/4/4/044013, 2009.

Dall'Osto, M., Harrison, R. M., Highwood, E. J., O'Dowd, C., Ceburnis, D., Querol, X. and Achterberg, E. P.: Variation of the mixing state of Saharan dust particles with atmospheric transport, Atmos. Environ., 44(26), 3135–3146, doi:https://doi.org/10.1016/j.atmosenv.2010.05.030, 2010.

Delany, A. C. and Zenchelsky, S.: THE ORGANIC COMPONENT OF WIND-EROSION-GENERATED SOIL-DERIVED AEROSOL, Soil Sci., 121(3) [online] Available from: https://journals.lww.com/soilsci/Fulltext/1976/03000/THE_ORGANIC_COMPONENT_OF_WIND_EROSION_GENERATED.2.aspx, 1976.

Demott, P. J., Prenni, A. J., Mcmeeking, G. R., Sullivan, R. C., Petters, M. D., Tobo, Y., Niemand, M., Möhler, O., Snider, J. R., Wang, Z. and Kreiden: Integrating laboratory and field data to quantify the immersion freezing ice nucleation activity of mineral dust particles, , 393–409, doi:10.5194/acp-15-393-2015, 2015.

DeMott, P. J., Hill, T. C. J., McCluskey, C. S., Prather, K. A., Collins, D. B., Sullivan, R. C., Ruppel, M. J., Mason, R. H., Irish, V. E., Lee, T., Hwang, C. Y., Rhee, T. S., Snider, J. R., McMeeking, G. R., Dhaniyala, S., Lewis, E. R., Wentzell, J. J. B., Abbatt, J., Lee, C., Sultana, C. M., Ault, A. P., Axson, J. L., Diaz Martinez, M., Venero, I., Santos-Figueroa, G., Stokes, M. D., Deane, G. B., Mayol-Bracero, O. L., Grassian, V. H., Bertram, T. H., Bertram, A. K., Moffett, B. F. and Franc, G. D.: Sea spray aerosol as a unique source of ice nucleating particles, Proc. Natl. Acad. Sci., 113(21), 5797–5803, doi:10.1073/pnas.1514034112, 2016.

DeMott, P. J., Hill, T. C. J., Petters, M. D., Bertram, A. K., Tobo, Y., Mason, R. H., Suski, K. J., Mccluskey, C. S., Levin, E. J. T., Schill, G. P., Boose, Y., Rauker, A. M., Miller, A. J., Zaragoza, J., Rocci, K., Rothfuss, N. E., Taylor, H. P., Hader, J. D., Chou, C., Huffman, J. A., Pöschl, U., Prenni, A. J. and Kreidenweis, S. M.: Comparative measurements of ambient atmospheric concentrations of ice nucleating particles using multiple immersion freezing methods and a continuous flow diffusion chamber, Atmos. Chem. Phys., 17(18), 11227–11245, doi:10.5194/acp-17-11227-2017, 2017.

DeMott, P. J., Möhler, O., Cziczo, D. J., Hiranuma, N., Petters, M. D., Petters, S. S., Belosi, F., Bingemer, H. G., Brooks, S. D., Budke, C., Burkert-Kohn, M., Collier, K. N., Danielczok, A., Eppers, O., Felgitsch, L., Garimella, S., Grothe, H., Herenz, P., Hill, T. C. J., Höhler, K., Kanji, Z. A., Kiselev, A., Koop, T., Kristensen, T. B., Krüger, K., Kulkarni, G., Levin, E. J. T., Murray, B. J., Nicosia, A., O'Sullivan, D., Peckhaus, A., Polen, M. J., Price, H. C., Reicher, N., Rothenberg, D. A., Rudich, Y., Santachiara, G., Schiebel, T., Schrod, J., Seifried, T. M., Stratmann, F., Sullivan, R. C., Suski, K. J., Szakáll, M., Taylor, H. P., Ullrich, R., Vergara-Temprado, J., Wagner, R., Whale, T. F., Weber, D., Welti, A., Wilson, T. W., Wolf, M. J. and Zenker, J.: The Fifth International Workshop on Ice Nucleation phase 2 (FIN-02): laboratory intercomparison of ice nucleation measurements, Atmos. Meas. Tech., 11(11), 6231–6257, doi:10.5194/amt-11-6231-2018, 2018.

Eastwood, M. L., Cremel, S., Wheeler, M., Murray, B. J., Girard, E. and Bertram, A. K.: Effects of sulfuric acid and ammonium sulfate coatings on the ice nucleation properties of kaolinite particles, Geophys. Res. Lett., 36(2), doi:https://doi.org/10.1029/2008GL035997, 2009.

Edtbauer, A., Stönner, C., Pfannerstill, E. Y., Berasategui, M., Walter, D., Crowley, J. N., Lelieveld, J. and Williams, J.: A new marine biogenic emission: methane sulfonamide (MSAM), dimethyl sulfide (DMS), and dimethyl sulfone (\chem{DMSO_{2}}) measured in air over the Arabian Sea, Atmos. Chem. Phys., 20(10), 6081–6094, doi:10.5194/acp-20-6081-2020, 2020.

Eger, P. G., Friedrich, N., Schuladen, J., Shenolikar, J., Fischer, H., Tadic, I., Harder, H., Martinez, M., Rohloff, R., Tauer, S., Drewnick, F., Fachinger, F., Brooks, J., Darbyshire, E., Sciare, J., Pikridas, M., Lelieveld, J. and Crowley, J. N.: Shipborne measurements of ClNO$_{2}$ in the Mediterranean Sea and around the Arabian Peninsula during summer, Atmos. Chem. Phys., 19(19), 12121–12140, doi:10.5194/acp-19-12121-2019, 2019.

Fennelly, M. J., Sewell, G., Prentice, M. B., O'Connor, D. J. and Sodeau, J. R.: Review: The Use of Real-Time Fluorescence Instrumentation to Monitor Ambient Primary Biological Aerosol Particles (PBAP), Atmosphere (Basel)., 9(1), doi:10.3390/atmos9010001, 2018.

Friedrich, N., Eger, P., Shenolikar, J., Sobanski, N., Schuladen, J., Dienhart, D., Hottmann, B., Tadic, I., Fischer, H., Martinez, M., Rohloff, R., Tauer, S., Harder, H., Pfannerstill, E. Y., Wang, N., Williams, J., Brooks, J., Drewnick, F., Su, H., Li, G., Cheng, Y., Lelieveld, J. and Crowley, J. N.: Reactive nitrogen around the Arabian Peninsula and in the Mediterranean Sea during the 2017 AQABA ship campaign, Atmos. Chem. Phys., 21(10), 7473–7498, doi:10.5194/acp-21-7473-2021, 2021.

Gandham, H., Dasari, H. P., Langodan, S., Karumuri, R. K. and Hoteit, I.: Major Changes in Extreme

1105 Dust Events Dynamics Over the Arabian Peninsula During 2003–2017 Driven by Atmospheric
1106 Conditions, J. Geophys. Res. Atmos., 125(24), e2020JD032931,
1107 doi:https://doi.org/10.1029/2020JD032931, 2020.

1108 Gelaro, R., McCarty, W., Suárez, M. J., Todling, R., Molod, A., Takacs, L., Randles, C. A., Darmenov,
1109 A., Bosilovich, M. G., Reichle, R., Wargan, K., Coy, L., Cullather, R., Draper, C., Akella, S., Buchard,
1110 V., Conaty, A., da Silva, A. M., Gu, W., Kim, G.-K., Koster, R., Lucchesi, R., Merkova, D., Nielsen, J.
1111 E., Partyka, G., Pawson, S., Putman, W., Rienecker, M., Schubert, S. D., Sienkiewicz, M. and Zhao, B.:
1112 The Modern-Era Retrospective Analysis for Research and Applications, Version 2 (MERRA-2), J. Clim.,
1113 30(14), 5419–5454, doi:10.1175/JCLI-D-16-0758.1, 2017.

1114 Gong, X., Wex, H., Müller, T., Wiedensohler, A., Höhler, K., Kandler, K., Ma, N., Dietel, B., Schiebel,
1115 T., Möhler, O. and Stratmann, F.: Characterization of aerosol properties at Cyprus, focusing on cloud
1116 condensation nuclei and ice-nucleating particles, Atmos. Chem. Phys., 19(16), 10883–10900,
1117 doi:10.5194/acp-19-10883-2019, 2019a.

1118 Gong, X., Wex, H., van Pinxteren, M., Triesch, N., Fomba, K. W., Lubitz, J., Stolle, C., Robinson, T.-B.,
1119 Müller, T., Herrmann, H. and Stratmann, F.: Ice nucleating particles measured in air, cloud and seawater
1120 at the Cape Verde Atmospheric Observatory (CVAO), , doi:10.1594/PANGAEA.906946, 2019b.

1121 Gong, X., Wex, H., van Pinxteren, M., Triesch, N., Fomba, K. W., Lubitz, J., Stolle, C., Robinson, T.-B.,
1122 Müller, T., Herrmann, H. and Stratmann, F.: Characterization of aerosol particles at Cabo Verde close to
1123 sea level and at the cloud level -- Part 2: Ice-nucleating particles in air, cloud and seawater, Atmos. Chem.
1124 Phys., 20(3), 1451–1468, doi:10.5194/acp-20-1451-2020, 2020.

1125 Hara, K., Maki, T., Kakikawa, M., Kobayashi, F. and Matsuki, A.: Effects of different temperature
1126 treatments on biological ice nuclei in snow samples, Atmos. Environ., 140, 415–419,
1127 doi:10.1016/j.atmosenv.2016.06.011, 2016.

1128 Harrison, A. D., Whale, T. F., Carpenter, M. A., Holden, M. A., Neve, L., O'Sullivan, D., Vergara
1129 Temprado, J. and Murray, B. J.: Not all feldspars are equal: a survey of ice nucleating properties across
1130 the feldspar group of minerals, Atmos. Chem. Phys., 16(17), 10927–10940, doi:10.5194/acp-16-10927-
1131 2016, 2016.

1132 Harrison, A. D., Lever, K., Sanchez-Marroquin, A., Holden, M. A., Whale, T. F., Tarn, M. D., McQuaid,
1133 J. B. and Murray, B. J.: The ice-nucleating ability of quartz immersed in water and its atmospheric
1134 importance compared to K-feldspar, Atmos. Chem. Phys., 19(17), 11343–11361, doi:10.5194/acp-19-
1135 11343-2019, 2019.

Hartmann, M., Adachi, K., Eppers, O., Haas, C., Herber, A., Holzinger, R., Hünerbein, A., Jäkel, E., Jentzsch, C., van Pinxteren, M., Wex, H., Willmes, S. and Stratmann, F.: Wintertime Airborne Measurements of Ice Nucleating Particles in the High Arctic: A Hint to a Marine, Biogenic Source for Ice Nucleating Particles, Geophys. Res. Lett., 47(13), e2020GL087770, doi:https://doi.org/10.1029/2020GL087770, 2020.

Hill, T. C. J., DeMott, P. J., Tobo, Y., Fröhlich-Nowoisky, J., Moffett, B. F., Franc, G. D. and Kreidenweis, S. M.: Sources of organic ice nucleating particles in soils, Atmos. Chem. Phys., 16(11), 7195–7211, doi:10.5194/acp-16-7195-2016, 2016.

Hinz, K.-P., Trimborn, A., Weingartner, E., Henning, S., Baltensperger, U. and Spengler, B.: Aerosol single particle composition at the Jungfraujoch, J. Aerosol Sci., 36(1), 123–145, doi:https://doi.org/10.1016/j.jaerosci.2004.08.001, 2005.

Hiranuma, N., Augustin-Bauditz, S., Bingemer, H., Budke, C., Curtius, J., Danielczok, A., Diehl, K., Dreischmeier, K., Ebert, M., Frank, F., Hoffmann, N., Kandler, K., Kiselev, A., Koop, T., Leisner, T., Möhler, O., Nillius, B., Peckhaus, A., Rose, D., Weinbruch, S., Wex, H., Boose, Y., DeMott, P. J., Hader, J. D., Hill, T. C. J., Kanji, Z. A., Kulkarni, G., Levin, E. J. T., McCluskey, C. S., Murakami, M., Murray, B. J., Niedermeier, D., Petters, M. D., O'Sullivan, D., Saito, A., Schill, G. P., Tajiri, T., Tolbert, M. A., Welti, A., Whale, T. F., Wright, T. P. and Yamashita, K.: A comprehensive laboratory study on the immersion freezing behavior of illite NX particles: a comparison of 17 ice nucleation measurement techniques, Atmos. Chem. Phys., 15(5), 2489–2518, doi:10.5194/acp-15-2489-2015, 2015.

Hoose, C. and Möhler, O.: Heterogeneous ice nucleation on atmospheric aerosols: A review of results from laboratory experiments., 2012.

Hoose, C., Kristjánsson, J. E., Chen, J.-P. and Hazra, A.: A Classical-Theory-Based Parameterization of Heterogeneous Ice Nucleation by Mineral Dust, Soot, and Biological Particles in a Global Climate Model, J. Atmos. Sci., 67(8), 2483–2503, doi:10.1175/2010JAS3425.1, 2010.

Huffman, J. A., Perring, A. E., Savage, N. J., Clot, B., Crouzy, B., Tummon, F., Shoshanim, O., Damit, B., Schneider, J., Sivaprakasam, V., Zawadowicz, M. A., Crawford, I., Gallagher, M., Topping, D., Doughty, D. C., Hill, S. C. and Pan, Y.: Real-time sensing of bioaerosols: Review and current perspectives, Aerosol Sci. Technol., 54(5), 465–495, doi:10.1080/02786826.2019.1664724, 2020.

Huneeus, N., Schulz, M., Balkanski, Y., Griesfeller, J., Prospero, J., Kinne, S., Bauer, S., Boucher, O., Chin, M., Dentener, F., Diehl, T., Easter, R., Fillmore, D., Ghan, S., Ginoux, P., Grini, A., Horowitz, L., Koch, D., Krol, M. C., Landing, W., Liu, X., Mahowald, N., Miller, R., Morcrette, J.-J., Myhre, G.,

Penner, J., Perlwitz, J., Stier, P., Takemura, T. and Zender, C. S.: Global dust model intercomparison in AeroCom phase I, Atmos. Chem. Phys., 11(15), 7781–7816, doi:10.5194/acp-11-7781-2011, 2011.

Kanji, Z. A., Ladino, L. A., Wex, H., Boose, Y., Burkert-Kohn, M., Cziczo, D. J. and Krämer, M.: Overview of Ice Nucleating Particles, Meteorol. Monogr., 58, 1.1-1.33, doi:10.1175/amsmonographs-d-16-0006.1, 2017.

Khaniabadi, Y. O., Daryanoosh, S. M., Amrane, A., Polosa, R., Hopke, P. K., Goudarzi, G., Mohammadi, M. J., Sicard, P. and Armin, H.: Impact of Middle Eastern Dust storms on human health, Atmos. Pollut. Res., 8(4), 606–613, doi:https://doi.org/10.1016/j.apr.2016.11.005, 2017.

Kinne, S., Schulz, M., Textor, C., Guibert, S., Balkanski, Y., Bauer, S. E., Berntsen, T., Berglen, T. F., Boucher, O., Chin, M., Collins, W., Dentener, F., Diehl, T., Easter, R., Feichter, J., Fillmore, D., Ghan, S., Ginoux, P., Gong, S., Grini, A., Hendricks, J., Herzog, M., Horowitz, L., Isaksen, I., Iversen, T., Kirkevåg, A., Kloster, S., Koch, D., Kristjansson, J. E., Krol, M., Lauer, A., Lamarque, J. F., Lesins, G., Liu, X., Lohmann, U., Montanaro, V., Myhre, G., Penner, J., Pitari, G., Reddy, S., Seland, O., Stier, P., Takemura, T. and Tie, X.: An AeroCom initial assessment – optical properties in aerosol component modules of global models, Atmos. Chem. Phys., 6(7), 1815–1834, doi:10.5194/acp-6-1815-2006, 2006.

Kleist, D. T., Parrish, D. F., Derber, J. C., Treadon, R., Wu, W.-S. and Lord, S.: Introduction of the GSI into the NCEP Global Data Assimilation System, Weather Forecast., 24(6), 1691–1705, doi:10.1175/2009WAF2222201.1, 2009.

Klingmüller, K., Pozzer, A., Metzger, S., Stenchikov, G. L. and Lelieveld, J.: Aerosol optical depth trend over the Middle East, Atmos. Chem. Phys., 16(8), 5063–5073, doi:10.5194/acp-16-5063-2016, 2016.

Knopf, D. A. and Koop, T.: Heterogeneous nucleation of ice on surrogates of mineral dust, J. Geophys. Res. Atmos., 111(D12), doi:https://doi.org/10.1029/2005JD006894, 2006.

Kok, J. F., Adebiyi, A. A., Albani, S., Balkanski, Y., Checa-Garcia, R., Chin, M., Colarco, P. R., Hamilton, D. S., Huang, Y., Ito, A., Klose, M., Li, L., Mahowald, N. M., Miller, R. L., Obiso, V., Pérez Garc\'\ia-Pando, C., Rocha-Lima, A. and Wan, J. S.: Contribution of the world's main dust source regions to the global cycle of desert dust, Atmos. Chem. Phys., 21(10), 8169–8193, doi:10.5194/acp-21-8169-2021, 2021.

Könemann, T., Savage, N., Klimach, T., Walter, D., Fröhlich-Nowoisky, J., Su, H., Pöschl, U., Huffman, J. A. and Pöhlker, C.: Spectral Intensity Bioaerosol Sensor (SIBS): an instrument for spectrally resolved fluorescence detection of single particles in real time, Atmos. Meas. Tech., 12(2), 1337–1363, doi:10.5194/amt-12-1337-2019, 2019.

1198 Krasnov, H., Katra, I. and Friger, M.: Increase in dust storm related PM10 concentrations: A time series
1199 analysis of 2001–2015, Environ. Pollut., 213, 36–42, doi:https://doi.org/10.1016/j.envpol.2015.10.021,
1200 2016.

1201 Krueger, B. J., Grassian, V. H., Cowin, J. P. and Laskin, A.: Heterogeneous chemistry of individual
1202 mineral dust particles from different dust source regions: the importance of particle mineralogy, Atmos.
1203 Environ., 38(36), 6253–6261, doi:https://doi.org/10.1016/j.atmosenv.2004.07.010, 2004.

1204 Krzywinski, M. and Altman, N.: Error bars, Nat. Methods, 10(10), 921–922, doi:10.1038/nmeth.2659,
1205 2013.

1206 Ladino, L. A., Raga, G. B., Alvarez-Ospina, H., Andino-Enr\'\iquez, M. A., Rosas, I., Mart\'\inez, L.,
1207 Salinas, E., Miranda, J., Ram\'\irez-D\'\iaz, Z., Figueroa, B., Chou, C., Bertram, A. K., Quintana, E. T.,
1208 Maldonado, L. A., Garc\'\ia-Reynoso, A., Si, M. and Irish, V. E.: Ice-nucleating particles in a coastal
1209 tropical site, Atmos. Chem. Phys., 19(9), 6147–6165, doi:10.5194/acp-19-6147-2019, 2019.

1210 Lohmann, U. and Feichter, J.: Global indirect aerosol effects: a review, Atmos. Chem. Phys., 5(3), 715–
1211 737, doi:10.5194/acp-5-715-2005, 2005.

1212 Manders, A. M. ., Schapp, M., Jozwicka, M., van Arkel, F., Weijers, E. . and Matthijsen, J.: The
1213 contribution of sea salt to PM 10 and PM in the Netherlands, [online] Available from:
1214 http://www.pbl.nl/sites/default/files/cms/publicaties/500099004.pdf, 2009.

1215 Martin, A. C., Cornwell, G., Beall, C. M., Cannon, F., Reilly, S., Schaap, B., Lucero, D., Creamean, J.,
1216 Ralph, F. M., Mix, H. T. and Prather, K.: Contrasting local and long-range-transported warm ice-
1217 nucleating particles during an atmospheric river in coastal California, USA, Atmos. Chem. Phys., 19(7),
1218 4193–4210, doi:10.5194/acp-19-4193-2019, 2019.

1219 Mayol, E., Jiménez, M. A., Herndl, G. J., Duarte, C. M. and Arrieta, J. M.: Resolving the abundance and
1220 air-sea fluxes of airborne microorganisms in the North Atlantic Ocean, Front. Microbiol., 5, 557,
1221 doi:10.3389/fmicb.2014.00557, 2014.

1222 McCluskey, C. S., Hill, T. C. J., Malfatti, F., Sultana, C. M., Lee, C., Santander, M. V, Beall, C. M.,
1223 Moore, K. A., Cornwell, G. C., Collins, D. B., Prather, K. A., Jayarathne, T., Stone, E. A., Azam, F.,
1224 Kreidenweis, S. M. and DeMott, P. J.: A Dynamic Link between Ice Nucleating Particles Released in
1225 Nascent Sea Spray Aerosol and Oceanic Biological Activity during Two Mesocosm Experiments, J.
1226 Atmos. Sci., 74(1), 151–166, doi:10.1175/JAS-D-16-0087.1, 2017.

1227 McCluskey, C. S., Hill, T. C. J., Sultana, C. M., Laskina, O., Trueblood, J., Santander, M. V., Beall, C.

M., Michaud, J. M., Kreidenweis, S. M., Prather, K. A., Grassian, V., DeMott, P. J., McCluskey, C. S., Hill, T. C. J., Sultana, C. M., Laskina, O., Trueblood, J., Santander, M. V., Beall, C. M., Michaud, J. M., Kreidenweis, S. M., Prather, K. A., Grassian, V. and DeMott, P. J.: A mesocosm double feature: Insights into the chemical make-up of marine ice nucleating particles, J. Atmos. Sci., JAS-D-17-0155.1, doi:10.1175/JAS-D-17-0155.1, 2018a.

McCluskey, C. S., Hill, T. C. J., Sultana, C. M., Laskina, O., Trueblood, J., Santander, M. V, Beall, C. M., Michaud, J. M., Kreidenweis, S. M., Prather, K. A., Grassian, V. and DeMott, P. J.: A Mesocosm Double Feature: Insights into the Chemical Makeup of Marine Ice Nucleating Particles, J. Atmos. Sci., 75(7), 2405–2423, doi:10.1175/JAS-D-17-0155.1, 2018b.

McCluskey, C. S., Ovadnevaite, J., Rinaldi, M., Atkinson, J., Belosi, F., Ceburnis, D., Marullo, S., Hill, T. C. J., Lohmann, U., Kanji, Z. A., O'Dowd, C., Kreidenweis, S. M. and DeMott, P. J.: Marine and Terrestrial Organic Ice-Nucleating Particles in Pristine Marine to Continentally Influenced Northeast Atlantic Air Masses, J. Geophys. Res. Atmos., 123(11), 6196–6212, doi:10.1029/2017JD028033, 2018c.

McCluskey, C. S., Hill, T. C. J., Humphries, R. S., Rauker, A. M., Moreau, S., Strutton, P. G., Chambers, S. D., Williams, A. G. and McRobert, I.: Observations of Ice Nucleating Particles Over Southern Ocean Waters, Geophys. Res. Lett., 989–997, doi:10.1029/2018GL079981, 2018d.

Megahed, K., 2007: The impact of mineral dust aerosol particles on cloud formation. Ph.D. dissertation, Rheinische Friedrich-Wilhelms-University Bonn, 175 pp. [Available online at https://bonndoc.ulb.uni-bonn.de/xmlui/handle/20.500.11811/3083]

Mitts, B., Wang, X., Lucero, D., Beall, C., Deane, G., DeMott, P. and Prather, K.: Importance of Supermicron Ice Nucleating Particles in Nascent Sea Spray, Geophys. Res. Lett., n/a(n/a), e2020GL089633, doi:https://doi.org/10.1029/2020GL089633, 2021.

Molod, A., Takacs, L., Suarez, M. and Bacmeister, J.: Development of the GEOS-5 atmospheric general circulation model: evolution from MERRA to MERRA2, Geosci. Model Dev., 8(5), 1339–1356, doi:10.5194/gmd-8-1339-2015, 2015.

Murray, B. J., O'Sullivan, D., Atkinson, J. D. and Webb, M. E.: Ice nucleation by particles immersed in supercooled cloud droplets., Chem. Soc. Rev., 41(19), 6519–54, doi:10.1039/c2cs35200a, 2012.

Nickovic, S., Vukovic, A., Vujadinovic, M., Djurdjevic, V. and Pejanovic, G.: Technical Note: High-resolution mineralogical database of dust-productive soils for atmospheric dust modeling, Atmos. Chem. Phys., 12(2), 845–855, doi:10.5194/acp-12-845-2012, 2012.

Formatted: Font: (Default) Times New Roman

Formatted: Font: (Default) Times New Roman

Formatted: Font: (Default) Times New Roman

Niedermeier, D., Augustin-Bauditz, S., Hartmann, S., Wex, H., Ignatius, K. and Stratmann, F.: Can we define an asymptotic value for the ice active surface site density for heterogeneous ice nucleation?, J. Geophys. Res. Atmos., 120(10), 5036–5046, doi:https://doi.org/10.1002/2014JD022814, 2015.

Niemand, M., Möhler, O., Vogel, B., Vogel, H., Hoose, C., Connolly, P., Klein, H., Bingemer, H., Demott, P., Skrotzki, J. and Leisner, T.: A particle-surface-area-based parameterization of immersion freezing on desert dust particles, J. Atmos. Sci., 69(10), 3077–3092, doi:10.1175/JAS-D-11-0249.1, 2012.

Nortcliff, S.: World Soil Resources and Food Security. Edited by R. Lal and BA Stewart. Boca Raton, Fl, USA: CRC Press (2012), pp. 574,£82.00. ISBN-13: 978-1439844502., Exp. Agric., 48(2), 305–306, 2012.

O'Sullivan, D., Murray, B. J., Malkin, T. L., Whale, T. F., Umo, N. S., Atkinson, J. D., Price, H. C., Baustian, K. J., Browse, J. and Webb, M. E.: Ice nucleation by fertile soil dusts: relative importance of mineral and biogenic components, Atmos. Chem. Phys., 14(4), 1853–1867, doi:10.5194/acp-14-1853-2014, 2014.

O'Sullivan, D., Adams, M. P., Tarn, M. D., Harrison, A. D., Vergara-Temprado, J., Porter, G. C. E., Holden, M. A., Sanchez-Marroquin, A., Carotenuto, F., Whale, T. F., McQuaid, J. B., Walshaw, R., Hedges, D. H. P., Burke, I. T., Cui, Z. and Murray, B. J.: Contributions of biogenic material to the atmospheric ice-nucleating particle population in North Western Europe, Sci. Rep., 8(1), 13821, doi:10.1038/s41598-018-31981-7, 2018.

Paramonov, M., David, R. O., Kretzschmar, R. and Kanji, Z. A.: A laboratory investigation of the ice nucleation efficiency of three types of mineral and soil dust, Atmos. Chem. Phys., 18(22), 16515–16536, doi:10.5194/acp-18-16515-2018, 2018.

Van Pelt, R. S. and Zobeck, T. M.: Chemical Constituents of Fugitive Dust, Environ. Monit. Assess., 130(1), 3–16, doi:10.1007/s10661-006-9446-8, 2007.

Perkins, R. J., Gillette, S. M., Hill, T. C. J. and DeMott, P. J.: The Labile Nature of Ice Nucleation by Arizona Test Dust, ACS Earth Sp. Chem., 4(1), 133–141, doi:10.1021/acsearthspacechem.9b00304, 2020.

Pfannerstill, E. Y., Wang, N., Edtbauer, A., Bourtsoukidis, E., Crowley, J. N., Dienhart, D., Eger, P. G., Ernle, L., Fischer, H., Hottmann, B., Paris, J.-D., Stönner, C., Tadic, I., Walter, D., Lelieveld, J. and Williams, J.: Shipborne measurements of total OH reactivity around the Arabian Peninsula and its role in ozone chemistry, Atmos. Chem. Phys., 19(17), 11501–11523, doi:10.5194/acp-19-11501-2019, 2019.

Price, H. C., Baustian, K. J., McQuaid, J. B., Blyth, A., Bower, K. N., Choularton, T., Cotton, R. J., Cui, Z., Field, P. R., Gallagher, M., Hawker, R., Merrington, A., Miltenberger, A., Neely III, R. R., Parker, S. T., Rosenberg, P. D., Taylor, J. W., Trembath, J., Vergara-Temprado, J., Whale, T. F., Wilson, T. W., Young, G. and Murray, B. J.: Atmospheric Ice-Nucleating Particles in the Dusty Tropical Atlantic, J. Geophys. Res. Atmos., 123(4), 2175–2193, doi:https://doi.org/10.1002/2017JD027560, 2018.

Prodi, F., Santachiara, G. and Oliosi, F.: Characterization of aerosols in marine environments (Mediterranean, Red Sea, and Indian Ocean), J. Geophys. Res. Ocean., 88(C15), 10957–10968, doi:https://doi.org/10.1029/JC088iC15p10957, 1983.

Rienecker, M. M., Suarez, M. J., Gelaro, R., Todling, R., Bacmeister, J., Liu, E., Bosilovich, M. G., Schubert, S. D., Takacs, L., Kim, G.-K., Bloom, S., Chen, J., Collins, D., Conaty, A., da Silva, A., Gu, W., Joiner, J., Koster, R. D., Lucchesi, R., Molod, A., Owens, T., Pawson, S., Pegion, P., Redder, C. R., Reichle, R., Robertson, F. R., Ruddick, A. G., Sienkiewicz, M. and Woollen, J.: MERRA: NASA's Modern-Era Retrospective Analysis for Research and Applications, J. Clim., 24(14), 3624–3648, doi:10.1175/JCLI-D-11-00015.1, 2011.

Salam, A., Lohmann, U. and Lesins, G.: Ice nucleation of ammonia gas exposed montmorillonite mineral dust particles, Atmos. Chem. Phys., 7(14), 3923–3931, doi:10.5194/acp-7-3923-2007, 2007.

Schnell, R. C.: Ice Nuclei in Seawater, Fog Water and Marine Air off the Coast of Nova Scotia: Summer 1975, J. Atmos. Sci., 34(8), 1299–1305, doi:10.1175/1520-0469(1977)034<1299:INISFW>2.0.CO;2, 1977.

Schrod, J., Weber, D., Drücke, J., Keleshis, C., Pikridas, M., Ebert, M., Cvetković, B., Nickovic, S., Marinou, E., Baars, H., Ansmann, A., Vrekoussis, M., Mihalopoulos, N., Sciare, J., Curtius, J. and Bingemer, H. G.: Ice nucleating particles over the Eastern Mediterranean measured by unmanned aircraft systems, Atmos. Chem. Phys., 17(7), 4817–4835, doi:10.5194/acp-17-4817-2017, 2017.

Shahsavani, A., Naddafi, K., Jafarzade Haghighifard, N., Mesdaghinia, A., Yunesian, M., Nabizadeh, R., Arahami, M., Sowlat, M. H., Yarahmadi, M., Saki, H., Alimohamadi, M., Nazmara, S., Motevalian, S. A. and Goudarzi, G.: The evaluation of PM10, PM2.5, and PM1 concentrations during the Middle Eastern Dust (MED) events in Ahvaz, Iran, from april through september 2010, J. Arid Environ., 77, 72–83, doi:https://doi.org/10.1016/j.jaridenv.2011.09.007, 2012.

Sullivan, R. C., Guazzotti, S. A., Sodeman, D. A. and Prather, K. A.: Direct observations of the atmospheric processing of Asian mineral dust, Atmos. Chem. Phys., 7(5), 1213–1236, doi:10.5194/acp-7-1213-2007, 2007.

Sullivan, R. C., Miñambres, L., DeMott, P. J., Prenni, A. J., Carrico, C. M., Levin, E. J. T. and Kreidenweis, S. M.: Chemical processing does not always impair heterogeneous ice nucleation of mineral dust particles, Geophys. Res. Lett., 37(24), doi:https://doi.org/10.1029/2010GL045540, 2010a.

Sullivan, R. C., Petters, M. D., DeMott, P. J., Kreidenweis, S. M., Wex, H., Niedermeier, D., Hartmann, S., Clauss, T., Stratmann, F., Reitz, P., Schneider, J. and Sierau, B.: Irreversible loss of ice nucleation active sites in mineral dust particles caused by sulphuric acid condensation, Atmos. Chem. Phys., 10(23), 11471–11487, doi:10.5194/acp-10-11471-2010, 2010b.

Suski, K. J., Hill, T. C. J., Levin, E. J. T., Miller, A., DeMott, P. J. and Kreidenweis, S. M.: Agricultural harvesting emissions of ice-nucleating particles, Atmos. Chem. Phys., 18(18), 13755–13771, doi:10.5194/acp-18-13755-2018, 2018.

Tadic, I., Crowley, J. N., Dienhart, D., Eger, P., Harder, H., Hottmann, B., Martinez, M., Parchatka, U., Paris, J.-D., Pozzer, A., Rohloff, R., Schuladen, J., Shenolikar, J., Tauer, S., Lelieveld, J. and Fischer, H.: Net ozone production and its relationship to nitrogen oxides and volatile organic compounds in the marine boundary layer around the Arabian Peninsula, Atmos. Chem. Phys., 20(11), 6769–6787, doi:10.5194/acp-20-6769-2020, 2020.

Tobo, Y., DeMott, P. J., Hill, T. C. J., Prenni, A. J., Swoboda-Colberg, N. G., Franc, G. D. and Kreidenweis, S. M.: Organic matter matters for ice nuclei of agricultural soil origin, Atmos. Chem. Phys., 14(16), 8521–8531, doi:10.5194/acp-14-8521-2014, 2014.

Ullrich, R., Hoose, C., Möhler, O., Niemand, M., Wagner, R., Höhler, K., Hiranuma, N., Saathoff, H. and Leisner, T.: A new ice nucleation active site parameterization for desert dust and soot, J. Atmos. Sci., 74(3), 699–717, doi:10.1175/JAS-D-16-0074.1, 2017.

Vali, G.: Quantitative Evaluation of Experimental Results an the Heterogeneous Freezing Nucleation of Supercooled Liquids, J. Atmos. Sci., 28(3), 402–409, doi:10.1175/1520-0469(1971)028<0402:QEOERA>2.0.CO;2, 1971.

Vergara-Temprado, J., Murray, B. J., Wilson, T. W., O'Sullivan, D., Browse, J., Pringle, K. J., Ardon-Dryer, K., Bertram, A. K., Burrows, S. M., Ceburnis, D., Demott, P. J., Mason, R. H., O'Dowd, C. D., Rinaldi, M. and Carslaw, K. S.: Contribution of feldspar and marine organic aerosols to global ice nucleating particle concentrations, Atmos. Chem. Phys., 17(5), 3637–3658, doi:10.5194/acp-17-3637-2017, 2017.

Vergara-Temprado, J., Miltenberger, A. K., Furtado, K., Grosvenor, D. P., Shipway, B. J., Hill, A. A., Wilkinson, J. M., Field, P. R., Murray, B. J. and Carslaw, K. S.: Strong control of Southern Ocean cloud

reflectivity by ice-nucleating particles, Proc. Natl. Acad. Sci., 115(11), 2687 LP – 2692, doi:10.1073/pnas.1721627115, 2018.

Wang, N., Edtbauer, A., Stönner, C., Pozzer, A., Bourtsoukidis, E., Ernle, L., Dienhart, D., Hottmann, B., Fischer, H., Schuladen, J., Crowley, J. N., Paris, J.-D., Lelieveld, J. and Williams, J.: Measurements of carbonyl compounds around the Arabian Peninsula: overview and model comparison, Atmos. Chem. Phys., 20(18), 10807–10829, doi:10.5194/acp-20-10807-2020, 2020.

Wang, X., Deane, G. B., Moore, K. A., Ryder, O. S., Stokes, M. D., Beall, C. M., Collins, D. B., Santander, M. V, Burrows, S. M., Sultana, C. M. and Prather, K. A.: The role of jet and film drops in controlling the mixing state of submicron sea spray aerosol particles, Proc. Natl. Acad. Sci., 114(27), 6978–6983, doi:10.1073/pnas.1702420114, 2017.

von der Weiden, S.-L., Drewnick, F. and Borrmann, S.: Particle Loss Calculator – a new software tool for the assessment of the performance of aerosol inlet systems, Atmos. Meas. Tech., 2(2), 479–494, doi:10.5194/amt-2-479-2009, 2009.

Welti, A., Lüönd, F., Kanji, Z. A., Stetzer, O. and Lohmann, U.: Time dependence of immersion freezing: an experimental study on size selected kaolinite particles, Atmos. Chem. Phys., 12(20), 9893–9907, doi:10.5194/acp-12-9893-2012, 2012.

Wex, H., DeMott, P. J., Tobo, Y., Hartmann, S., Rösch, M., Clauss, T., Tomsche, L., Niedermeier, D. and Stratmann, F.: Kaolinite particles as ice nuclei: learning from the use of different kaolinite samples and different coatings, Atmos. Chem. Phys., 14(11), 5529–5546, doi:10.5194/acp-14-5529-2014, 2014.

Wex, H., Huang, L., Zhang, W., Hung, H., Traversi, R., Becagli, S., Sheesley, R. J., Moffett, C. E., Barrett, T. E., Bossi, R., Skov, H., Hünerbein, A., Lubitz, J., Löffler, M., Linke, O., Hartmann, M., Herenz, P. and Stratmann, F.: Annual variability of ice-nucleating particle concentrations at different Arctic locations, Atmos. Chem. Phys., 19(7), 5293–5311, doi:10.5194/acp-19-5293-2019, 2019.

Whale, T. F., Murray, B. J., O'Sullivan, D., Wilson, T. W., Umo, N. S., Baustian, K. J., Atkinson, J. D., Workneh, D. A. and Morris, G. J.: A technique for quantifying heterogeneous ice nucleation in microlitre supercooled water droplets, Atmos. Meas. Tech., 8(6), 2437–2447, doi:10.5194/amt-8-2437-2015, 2015.

Wilson, T. W., Ladino, L. a., Alpert, P. a., Breckels, M. N., Brooks, I. M., Browse, J., Burrows, S. M., Carslaw, K. S., Huffman, J. A., Judd, C., Kilthau, W. P., Mason, R. H., McFiggans, G., Miller, L. a., Nájera, J. J., Polishchuk, E., Rae, S., Schiller, C. L., Si, M., Temprado, J. V., Whale, T. F., Wong, J. P. S., Wurl, O., Yakobi-Hancock, J. D., Abbatt, J. P. D., Aller, J. Y., Bertram, A. K., Knopf, D. a. and Murray, B. J.: A marine biogenic source of atmospheric ice-nucleating particles, Nature, 525(7568), 234–238,

doi:10.1038/nature14986, 2015.

Wu, W.-S., Purser, R. J. and Parrish, D. F.: Three-Dimensional Variational Analysis with Spatially Inhomogeneous Covariances, Mon. Weather Rev., 130(12), 2905–2916, doi:10.1175/1520-0493(2002)130<2905:TDVAWS>2.0.CO;2, 2002.

Yadav, S., Venezia, R. E., Paerl, R. W. and Petters, M. D.: Characterization of Ice-Nucleating Particles Over Northern India, J. Geophys. Res. Atmos., 124(19), 10467–10482, doi:https://doi.org/10.1029/2019JD030702, 2019.

Yahya, R. Z., Arrieta, J. M., Cusack, M. and Duarte, C. M.: Airborne Prokaryote and Virus Abundance Over the Red Sea, Front. Microbiol., 10, 1112, doi:10.3389/fmicb.2019.01112, 2019.

Yang, J., Wang, Z., Heymsfield, A. J., DeMott, P. J., Twohy, C. H., Suski, K. J. and Toohey, D. W.: High ice concentration observed in tropical maritime stratiform mixed-phase clouds with top temperatures warmer than −8 °C, Atmos. Res., 233, 104719, doi:https://doi.org/10.1016/j.atmosres.2019.104719, 2020.

Yost, J. L. and Hartemink, A. E.: Chapter Four - Soil organic carbon in sandy soils: A review, vol. 158, edited by D. L. Sparks, pp. 217–310, Academic Press., 2019.

Yu, Y., Kalashnikova, O. V, Garay, M. J., Lee, H. and Notaro, M.: Identification and Characterization of Dust Source Regions Across North Africa and the Middle East Using MISR Satellite Observations, Geophys. Res. Lett., 45(13), 6690–6701, doi:https://doi.org/10.1029/2018GL078324, 2018.

Zolles, T., Burkart, J., Häusler, T., Pummer, B., Hitzenberger, R. and Grothe, H.: Identification of Ice Nucleation Active Sites on Feldspar Dust Particles, J. Phys. Chem. A, 119(11), 2692–2700, doi:10.1021/jp509839x, 2015.